

Ilia State University
Institute of Theoretical Physics
Center for Theoretical Astrophysics

with the rights of manuscript

Nino Chkheidze

**The plasma model of XDINS and Crab pulsar's HE
emission**

**Dissertation Presented in Partial Fulfilment of the Requirements
for the Degree of Doctor in Physics**

Supervisor: Professor Giorgi Machabeli

Co-supervisor: Professor Zaza Osmanov

Tbilisi, 2011

Abstract

In the present thesis a self-consistent theory is constructed, interpreting the observations of individual pulsars. The distribution function of relativistic electrons is one-dimensional and anisotropic at the pulsar surface and plasma becomes unstable, which can lead to wave excitation in the outer part of the pulsar magnetosphere. Generation of waves is possible if the condition of cyclotron resonance is fulfilled. During this process one also has a simultaneous feedback of excited waves on the resonant electrons. This mechanism is described by quasi-linear diffusion (QLD), leading to the diffusion of particles along and across the magnetic field lines. Consequently, resonant particles acquire perpendicular momenta and start to radiate in the synchrotron regime. On the basis of the Vlasov's kinetic equation we formulate the equations controlling such processes, and obtain the solution for this equations.

The measured X-ray spectra of RX J1856.5-3754 and RX J2143.0+0654 are explained under the assumption of a synchrotron mechanism. These objects are the nearby isolated neutron stars, and considerable observational resources have been devoted to them. However, current models are unable to satisfactorily explain the data. We show that our latest model, which is based on well-developed theory of pulsars represents the most self-consistent picture to date for explaining all the observations. We confirm that the cyclotron instability is quite efficient, since the estimations show that the time of wave-particle interaction is long enough for particles to acquire perpendicular momenta and generate observed radiation.

The present model provides simultaneous generation of low and high energy emission in one location of the pulsar magnetosphere. Relying on this fact, we suppose that generation of phase-aligned signals from different frequency bands of the Crab pulsar can be explained in the framework of the model. Particularly, here we investigate the recently detected high energy (HE) emission ($\sim 25\text{GeV}$) of the Crab pulsar and explain its coincidence with the radio pulses. A different approach of the synchrotron theory is considered, giving the spectral index of the HE emission ($\beta = 2$) and the exponential cutoff energy (23GeV) in a good agreement with the observational data.

Nomenclature

CDI	Curvature drift instability
GJ	Goldreich-Julian
HE	High energy
ICS	Inverse Compton scattering
NS	Neutron star
PA	Position angle
QLD	Quasi-linear diffusion
XDINS	X-ray dim isolated neutron stars

Contents

1	Introduction	3
1.1	XDINS	5
1.2	Crab pulsar	7
1.3	An outline of the thesis	11
2	The plasma emission model	12
2.1	Fundamental modes of electron-positron plasma	15
2.2	Cyclotron instability and its excitation conditions	18
2.3	The feedback of generated waves on the distribution of the resonant particles – the quasi-linear diffusion	21
3	Synchrotron emission	25
3.1	Synchrotron radiation of a single electron	26
3.2	Synchrotron spectrum of the set of electrons	28
3.2.1	The standard approach	28
3.2.2	The model	30
4	RX J1856.5-3754 and RX J2143.0+0654 (RBS1774)	35
4.1	X-ray spectral analysis	38
4.2	Possible nature of the spectral feature in the X-ray emission of RBS1774	42
4.3	Optical emission	44
4.4	The effectiveness of the cyclotron mechanism	45
4.5	The recently discovered 7s pulsations of RXJ1856	45

4.5.1	Generation of drift waves	46
4.5.2	Change of the field line curvature and the emission di- rection by the drift waves	48
4.5.3	The model	49
4.6	The polarization properties of RXJ1856	55
4.6.1	Emission polarization	56
4.6.2	Position angle	58
5	The HE energy pulsed emission of PSR B0531+21	60
5.1	Synchrotron HE spectrum of the Crab pulsar	61
5.2	Compton scattering	63
5.3	Curvature radiation	64
6	Discussion and Conclusions	67
	Appendix	73

Chapter 1

Introduction

The discovery of pulsars in 1967 by Hewish et al. (1968) was one of the most exciting events in the history of astronomy. Soon after their discovery pulsars were identified with rotating highly magnetized neutron stars, which emit beamed electromagnetic radiation that is powered by the rotational energy of the star (Gold, 1969). Due to the rotation of the pulsar, the emission appears to be pulsed for a distant observer. The extreme conditions existing in pulsars and their magnetosphere raised high interest of scientists. The surface magnetic fields are reaching $B \sim 10^{12} - 10^{13}\text{G}$, and the mass density inside the star is comparable to the nuclear density $\sim 10^{14} - 10^{15}\text{g cm}^{-3}$. Pulsar astronomers have now detected over 2000 pulsars and expect to discover thousands more during the next few years.

At present there are about 12 competing theories which differ both in the physical effects responsible for the pulsar emission and in the location where the radiation is generated. To date, the most widely discussed theory attributes the emission to coherent curvature emission by bunches of particles. Although this theory can explain a broad range of observed pulsar properties by the careful arrangement of the magnetic field geometry and the form and size of bunches, 30 years of theoretical efforts have failed to explain the origin of these bunches (Melrose, 1995). This theory can also be ruled out on observational grounds (Lesch et al., 1998). In addition to the work of Lesch et al. (1998) we note that this theory also fails to explain the observed correlations of the conal peaks (Kazbegi et al., 1991b) and the large size of the emitting region (Gwinn et al., 1997).

We propose that the pulsar emission is generated by plasma instabilities developing in the outflowing plasma on the open field lines of the pulsar magnetosphere. Plasma can be considered as an active medium that can amplify its normal modes. The wave amplification can be the result of the resonant wave-particle interaction, i.e. in the rest frame of the particle the frequency of the resonant wave is zero or a multiple of the gyration frequency. The plasma instabilities that we argue operate in the pulsar magnetosphere may be described by the (somewhat contradictory) term incoherent broad-band maser. Each single emission by a charged particle is a result of the stimulated, as opposed to spontaneous, emission process. Unlike conventional lasers in which basically one single frequency gets amplified, in this case charged particles can resonate with many mutually incoherent waves with different frequencies.

To explain the observed pulsar properties, we rely on the pulsar emission model first developed by Machabeli & Usov (1979) and Lominadze et al. (1983). It is well known that the distribution function of relativistic particles is one dimensional at the pulsar surface, because any transverse momenta (p_{\perp}) of relativistic electrons are lost in a very short time ($\leq 10^{-20}$ s) via synchrotron emission in very strong $B \sim 10^{12}$ G magnetic fields. This means that one needs a certain mechanism, leading to the creation of the pitch angles restoring the synchrotron radiation. The main mechanism of wave generation in plasmas of the pulsar magnetosphere is the cyclotron instability (Kazbegi et al., 1992). During the quasi-linear stage of the instability, a diffusion of particles arises along and across the magnetic field lines. Therefore, the resonant electrons acquire transverse momenta and, as a result start to radiate in the synchrotron regime. The original waves generated by the cyclotron resonance are vacuum-like electromagnetic waves, so they may leave the magnetosphere directly and reach an observer. These waves mainly come in the radio or optical domain and might be detected with higher frequency emission that is generated in the same area of the pulsar magnetosphere by synchrotron mechanism.

In a number of papers (Chkheidze & Machabeli, 2007; Chkheidze et al.,

2010; Chkheidze, 2011), we attempted to describe the emission spectra of individual pulsars under the assumption of a synchrotron mechanism, switched on the light cylinder length-scales (a hypothetical zone, where the linear velocity of rigid rotation exactly equals the speed of light), due to the QLD developed by means of the cyclotron instability. Particularly, in the framework of our emission model we investigated the observed properties of two members (RX J1856.5-3754 and RX J2143.0+0654) of the peculiar class of pulsars, the so called 'XDINS' - X-ray dim isolated neutron stars. We also explained the recently observed HE emission of the Crab pulsar. Let us make a brief overview of these objects.

1.1 XDINS

Over the last decade ROSAT observations have led to the discovery of seven very soft X-ray sources with quite particular characteristics, commonly called X-ray dim isolated neutron stars. They exhibit very similar properties and despite intensive searches their number remained constant since 2001. Identification of additional sources that may still be present (Rutledge et al., 2003) in the ROSAT Bright Sources Catalog (containing ≈ 18000 sources with > 0.05 counts s^{-1} with the Position-Sensitive Proportional Counter, or PSPC; Voges et al. (1999)) is extremely difficult given the poor positional accuracy of the PSPC.

Although it is now widely agreed that the seven ROSAT sources are isolated neutron stars, their puzzling properties make the origin of their emission still uncertain. The overall X-ray spectrum of XDINS is well reproduced by an absorbed blackbody with temperatures in the range $kT \sim 40 - 100$ eV. Consequently, it is mostly supposed that the emission of these sources have a thermal nature. The discovery of the seven neutron stars (which are often called the 'Magnificent Seven') with purely thermal X-ray spectra raised wide interest by theoreticians and observers as promising objects to learn about atmospheres and the internal structure of neutron stars (e.g. Paereles et al. (2001)). Hence, every effort is directed to making a thermal emission model

which would well describe the observational properties of XDINS. Application of more sophisticated, and physically motivated, models for the surface emission (atmospheric models in particular) result in worse agreement with the data. To explain this fact, it has been proposed¹ that the star has no atmosphere but a condensed matter surface. The mentioned surface might result in a virtually featureless Planckian spectrum in the soft X-ray band.

Detailed multiwavelength studies of XDINS are fundamental for tracking their evolutionary history, and for shedding light on their properties. While the XDINS have similar spectral properties in the X-rays, in the optical the paucity of multi-band observations prevents a clear spectral characterization. For the XDINS with a certified counterpart (see e.g. Kaplan (2008)) the optical emission lies typically a factor ~ 10 , or more, above the extrapolation of the X-ray blackbody into the optical/UV band. However, while the optical flux closely follows a Rayleigh-Jeans distribution in RX J1856.5-3754, possible deviations from a λ^{-4} behaviour have been reported for RX J0720.4-3125 and RX J1605.3+3249 ((Kaplan et al., 2003; Motch et al., 2003, 2005; Zane et al., 2006). Thus, whether the optical emission from XDINS is produced by regions of the star surface at a lower temperature (e.g. Pons et al. (2002)) or by other mechanisms, such as non-thermal emission from particles in the star magnetosphere or reprocessing of the surface radiation by an optically thin (to X-rays) hydrogen layer surrounding the star (Motch et al., 2003; Ho et al., 2007), is still under debate.

Since the broadband spectra of this sources cannot be fitted by a single Planckian spectrum, it is often described by two-temperature blackbody models (Pons et al., 2002; Pavlov, Zavlin & Sanwal, 2002; Burwitz et al., 2003). However, condensation of surface matter requires very specific conditions to be fulfilled (Lai & Salpeter, 1997; Lai, 2001). Even if these conditions are satisfied, the formation of a non-uniform distribution of the surface temperature (two-temperature blackbody models) still remains unclear. The most adequate fits of the spectra give models which assume that the star has a thin hydrogen atmosphere superposed on a condensed matter surface (Motch et

¹Originally suggested by G. Pavlov (2000)

al., 2003; Ho et al., 2007). But the origin of such thin hydrogen layers fitting the data is a problematic issue.

The only reason for the consideration that the XDINS are the sources of pure thermal radiation is that their X-ray spectra are best described by the Planckian function. The plasma emission model presented in this work explains the measured soft X-ray spectra of XDINS as well. We suggest that the X-ray radiation of these objects is generated by a synchrotron mechanism, switched on during the quasi-linear stage of the cyclotron instability. In particular, the X-ray spectra of RX J1856.5-3754 and RX J2143.0+0654 are as well fitted with the model spectrum, as with the Planckian one. The reason for this is that we consider a different approach of the synchrotron theory, which provides the synchrotron spectra that are not only power-law but also might contain the exponential cutoff. The current model gives successful explanation of observational data without facing problems typical of the thermal radiation models. However, the most reliable argument revealing the real emission nature of XDINS would be the study of these objects with future polarization instruments, such as Constellation-X, XEUS, and the Extreme Physics Explorer (Bellazini et al., 2006; Elvis, 2006; Jahoda et al., 2007).

1.2 Crab pulsar

The Crab Nebula is among the brightest objects of our Galaxy and it is the remnant of a supernova explosion that occurred in AD 1054 (e.g. Collins et al. (1999), and references therein) at a distance of ~ 2 kpc. It is one of the best studied non-thermal celestial objects in almost all wavelength bands of the electromagnetic spectrum from 10^{-5} eV (radio) to nearly 10^{14} eV (γ -rays). In very high energy γ -ray astronomy the Crab Nebula was first detected with large significance at TeV energies by the pioneering Whipple telescope (Weekes et al., 1989). The nebula turned out to be the strongest source of steady very high energy γ -ray emission in the Galaxy. It is therefore used as the standard 'calibration candle' for groundbased γ -ray experiments.

It has been ascertained that its energy can have only one source, a pulsar PSR B0531+21 (Crab pulsar) within the nebula, and that most of the Crab's radiation can be explained by synchrotron mechanism (Shklovsky, 1953; Dombrovsky, 1954; Vashakidze, 1954; Oort & Walraven, 1956). The Crab pulsar/Nebula system is one of the most intensely studied astrophysical sources with measurements throughout the electromagnetic spectrum from the radio to the TeV energy band. The similarity of the spectra of Crab Nebula and its pulsar in the HE domain suggests the unity of their radiation mechanisms.

In most regions of the spectrum, the characteristic 33ms pulsations of the pulsar are clearly visible. The pulse profile is unique among known pulsars in that it is aligned from radio to gamma-ray energies (Lessard et al., 2000). Investigations of last decade have shown that the aforementioned coincidence takes places in the HE domain (0.01MeV-25GeV) as well (Aliu et al., 2008). From 2007 October to 2008 February, the MAGIC Cherenkov telescope has discovered pulsed emission above 25GeV. The recent detection of HE γ -rays from the Crab pulsar could be very important (Aliu et al., 2008).

One of the fundamental problems concerning pulsars relates the origin of the HE electromagnetic radiation. According to the standard approach, two major mechanisms govern the HE radiation: the inverse Compton scattering (e.g. Blandford et al. (1990)) and the synchrotron emission (Paereles et al., 2001). On the other hand, up to now in most of the cases it is not clear where the location of the HE electromagnetic radiation is: closer to the pulsar (polar cap model, see for example Daugherty & Harding (1982)) or farther out in the magnetosphere (outer gap model, see for example Romani & Yadigaroglu (1995)). An exception is the HE emission recently detected by the MAGIC Cherenkov telescope (Aliu et al., 2008), which has revealed that the pulsed radiation above 25GeV is inconsistent with the polar cap models (due to the observational fact, that the emission region is located in the outer part of the pulsar magnetosphere). In the outer gap models the generation of the HE radiation happens in the outer gap region (e. g. Romani & Yadigaroglu (1995)), which does not contradict with the observational fact

that the emission happens far out in the magnetosphere, but to our knowledge there is no mechanism of generation of radio emission.

In the framework of these models, over the star's surface there is a vacuum gap with the electric field inside (Ruderman & Sutherland, 1975), which accelerates particles up to relativistic energies leading to the emission process. Unfortunately, energies of particles accumulated in the gap, are not enough to explain the observed radiation. To solve this problem several mechanisms have been proposed. For increasing the gap size, by Usov & Shabad (1985) the formation of positronium (electron-positron bound state) was considered. Another mechanism, leading to the enlargement of the gap zone was introduced by Arons & Scharleman (1979) and the approach was based on a process of rectifying of the magnetic field lines. This method was applied by Harding et al. (2008) for studying the high altitude radiation from the pulsar slot gaps. The authors consider a three-dimensional model of optical and γ -ray emission from the slot gap accelerator of a spin-powered pulsar and predict that the slot gap emission below 200MeV will exhibit correlations in time and phase with the radio emission. A general relativistic approach has been proposed by Muslimov & Tsygan (1992), where, taking into account the fact that in the vicinity of the NS (Neutron star), the space-time is curved, the authors applied the Kerr metric. It was shown that the gap size increases due to the general relativistic effects. All aforementioned mechanisms provide the required increase in the gap area, but it is not enough for explaining the observed radiation. These problems provoked a series of works considering the so-called outer gap models, where for studying emission from pulsars, several mechanisms have been proposed: the inverse Compton scattering, curvature radiation and the synchrotron emission.

In the present work we explain the HE radiation of the Crab pulsar relying on our plasma emission model. According to the work Chkheidze et al. (2010), in the electron-positron plasma of a pulsar magnetosphere the low frequency cyclotron modes, on the quasi-linear stage of their evolution create conditions for generation of the HE synchrotron emission. Therefore, generation of low and high frequency waves is a simultaneous process and it

takes place in one location of the pulsar magnetosphere (on the light cylinder lengthscales). Thus, in the framework of this model the coincidence of signals indicates that all frequencies having such properties are simultaneously generated in one location of the pulsar magnetosphere. This in turn, restricts possibility of choice of radiation mechanisms. It is clear that the inverse Compton scattering (ICS) or the curvature radiation cannot provide the observationally evident coincidence of signals, since they do not have any restriction on the spacial location of emission (area in the pulsar magnetosphere, where the corresponding radiation is produced). As it has been shown by Machabeli & Osmanov (2009, 2010), neither the curvature radiation nor the ICS may provide the above mentioned coincidence. In particular, analyzing the ICS, it has been demonstrated that for reasonable physical parameters even very energetic electrons are unable to produce the photon energies of the order of 25GeV. Studying the curvature radiation, it has been found that the curvature drift instability (see Osmanov et al., 2008; Osmanov et al., 2009b) efficiently rectifies the magnetic field lines making the role of the curvature emission process negligible (Machabeli & Osmanov, 2010).

1.3 An outline of the thesis

The Chapter 2 presents the model of the pulsar emission, that we use to explain the observed properties of individual pulsars. In Section 2.1 we consider the fundamental modes of the pair plasma and check the condition of their excitation on the cyclotron resonance. The cyclotron instability and its excitation conditions are investigated in Section 2.2 and the feedback of generated waves on the distribution of the resonant particles (QLD) is considered in Section 2.3.

In Chapter 3 the synchrotron emission theory is reviewed. Along with the standard theory we present our approach, which differs from the standard one, as it takes into account the mechanism of creation of the pitch-angles.

In Chapter 4 the plasma emission model is applied to the two members of XDINS: RX J1856.5-3754 and RX J2143.0+0654. It is demonstrated that the model well explains all the observational features and the fitting results of the X-ray data with the model are presented.

In Chapter 5 we apply the plasma model to explain the recently detected HE emission of the Crab pulsar. The observational fact of the coincidence of signals in low (radio) and HE domains is explained. Considering a new approach of the synchrotron theory based on our emission model, the spectral index, $\beta = 2$, of the HE emission is explained and the exponential cutoff, with the cutoff energy - 23GeV is obtained, being in a good agreement with the observational data. We also discuss other possible radiation mechanisms and demonstrate their unfitness with the observations.

In Chapter 6 we make conclusions and discuss our results.

Chapter 2

The plasma emission model

Any well known theory of pulsar emission suggests that, the observed radiation is generated due to processes taking place in electron-positron plasma. It is generally assumed that the pulsar magnetosphere is filled by dense relativistic electron-positron plasma flowing along the open magnetic field lines, which is generated as a consequence of the avalanche process first described by Goldreich & Julian (1969) and developed by Sturrock (1971) and Tademaru (1973). A spinning magnetized NS generates an electric field which extracts electrons from the star's surface and accelerates them to form a low density ($n_{b_0} = B_0/Pce$, where P is the pulsar rotation period and B_0 is the magnetic field at the star's surface) and energetic (the Lorentz factor of particles is $\gamma_b \sim 10^{6-8}$ for typical pulsars) primary beam. In a weakly curved magnetic field, electrons generate γ -quanta which in turn produce electron-positron pairs. The pitch angle of the particles which are produced is non-zero, so that secondary particles generate synchrotron radiation. This radiation in turn produces more pairs, and so on until the plasma becomes dense and screens the electric field. As a result a multicomponent plasma is formed, with an anisotropic one-dimensional distribution function (see Fig. 2.1 (Arons, 1981)), containing:

- (i) the bulk of plasma with an average Lorentz-factor $\gamma \sim \gamma_p$ and $n \sim n_p$;
- (ii) a high-energy 'tail' of the distribution function with $\gamma \sim \gamma_t$ and $n \sim n_t$;
- (iii) the primary beam with $\gamma \sim \gamma_b$ and $n \sim n_b$.

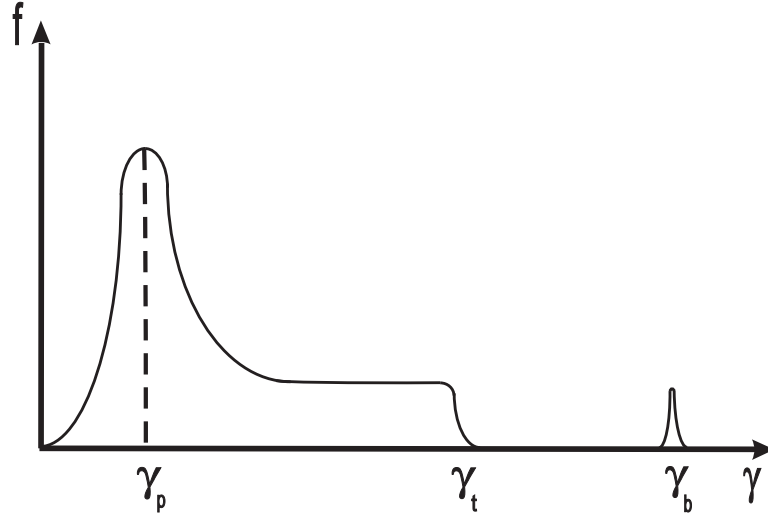


Figure 2.1: Distribution function of a one-dimensional plasma in the pulsar magnetosphere. Left corresponds to secondary particles, right to the primary beam.

We assume equipartition of energy among the plasma components

$$n_p \gamma_p \approx n_t \gamma_t \approx \frac{n_b \gamma_b}{2}. \quad (2.1)$$

The relativistic particles undergo drifting perpendicularly to the magnetic field due to the curvature, ρ , of the field lines. The corresponding drift velocity is given by

$$u_x = \frac{c V_\varphi \gamma_{res}}{\rho \omega_B}, \quad (2.2)$$

where V_φ is the component of velocity along the magnetic field lines and γ_{res} is the Lorentz factor of the resonant particles, $\omega_B \equiv eB/mc$ is the cyclotron frequency, e and m are the electron's charge and the rest mass, respectively and c is the speed of light.

The distribution function is one-dimensional and anisotropic and plasma becomes unstable, which can lead to excitation of the fundamental plasma modes in the pulsar magnetosphere (Sagdeev & Shafranov , 1960). Both of these factors (the one-dimensionality of the distribution function and the drift of particles) might cause generation of eigen modes in the electron-positron plasma if the following resonance condition is satisfied (Kazbegi et al., 1992)

$$\omega - k_\varphi V_\varphi - k_x u_x + \frac{s\omega_B}{\gamma_{res}} = 0, \quad (2.3)$$

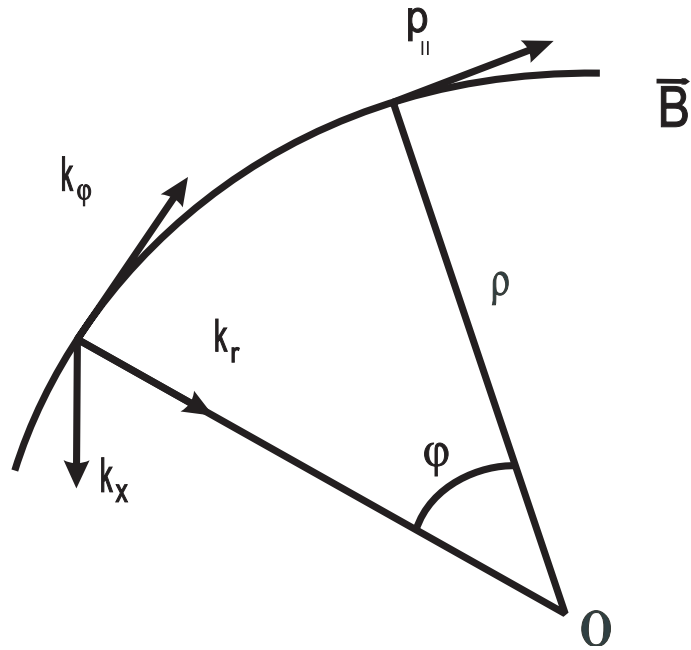


Figure 2.2: Cylindrical coordinate system (ρ is a local radius of curvature)

where $V_\varphi \approx c(1 - u_x^2/c^2 - 1/2\gamma_r^2)$, $k_\varphi^2 + k_\perp^2 = k^2$, $k_\perp^2 = k_x^2 + k_r^2$ and $s = 0, \pm 1, \pm 2, \dots$. Here a cylindrical coordinate system is chosen, with the x -axis directed perpendicular to the plane of the field lines, while r and φ are the radial and azimuthal coordinates (see Fig. 2.2). For $s = 0$ one has a hollow cone of the modified Cherenkov radiation (Kazbegi et al., 1992; Lyutikov et al., 1999a; Shapakhidze et al., 2003) and when $s = +1$ (the cyclotron resonance) one has the core emission, being a result of the anomalous Doppler effect.

To explain the observed emission of individual pulsars, we rely on the pulsar emission model first developed by Machabeli & Usov (1979) and Lominadze et al. (1979). According to these works, the main mechanism of wave generation in plasmas of the pulsar magnetosphere is the cyclotron instability, which develops on the light cylinder length-scales. Due to the cyclotron resonance, the low frequency cyclotron modes (which might be detected by an observer, as they are vacuum-like waves and can leave the magnetosphere directly), on the quasi-linear evolution stage of the instability create conditions for generation of the high energy synchrotron emission.

2.1 Fundamental modes of electron-positron plasma

It is essential to consider the eigen-modes of pair plasma, for studying the development of the cyclotron instability in the pulsar magnetosphere. The properties of a highly magnetized relativistic electron-positron plasma have been investigated quite thoroughly (Volokitin, Krasnoselskikh & Machabeli, 1985; Arons & Barnard, 1986; Lominadze et al., 1986). Differently from electron-ion plasma, in pair plasma gyrotropy is absent. Let us assume that the relative streaming of the plasma electrons and positrons

$$\Delta\gamma = \int \gamma f^+ d\gamma - \int \gamma f^- d\gamma \approx 0, \quad (2.4)$$

where f^- and f^+ are the one-dimensional distribution functions of electrons and positrons, which are normalized such that $\int f^\pm d\gamma = 1$. The distribution function of electrons is assumed to be identical with that of the positrons, in which case the dielectric tensor

$$\varepsilon_{ij} = \begin{pmatrix} \varepsilon_{11} & 0 & \varepsilon_{13} \\ 0 & \varepsilon_{22} & 0 \\ \varepsilon_{31} & 0 & \varepsilon_{33} \end{pmatrix}. \quad (2.5)$$

The Vlasov kinetic equation along with the Maxwell's equations in linear approximation give (Volokitin, Krasnoselskikh & Machabeli, 1985):

$$\begin{pmatrix} \frac{k_{\parallel}^2}{\omega^2} - \varepsilon_{11} & 0 & \frac{k_{\parallel}k_{\perp}c^2}{\omega^2} - \varepsilon_{13} \\ 0 & \frac{k_{\perp}^2c^2}{\omega^2} - \varepsilon_{22} & 0 \\ \frac{k_{\parallel}k_{\perp}c^2}{\omega^2} - \varepsilon_{31} & 0 & \frac{k_{\perp}^2}{\omega^2} - \varepsilon_{33} \end{pmatrix} \begin{pmatrix} E_1 \\ E_2 \\ E_3 \end{pmatrix} = 0, \quad (2.6)$$

where the electric field of waves is represented as

$$E = \frac{1}{2}E_0 \exp[i\vec{k}\vec{r} - i\omega t] + c.c. \quad (2.7)$$

The wave vector $\vec{k} = (k_{\perp}, 0, k_{\parallel})$, so that $k_{\perp} = k \sin \psi$ and $k_{\parallel} = k \cos \psi$ (ψ is the angle between the wave vector and the magnetic field). The waves propagating in such a plasma are only linearly polarized. The nonzero components

of the dielectric tensor have the form

$$\varepsilon_{11} = \varepsilon_{22} = 1 + \frac{\omega_p^2}{\omega} \int \frac{(\omega - k_{\parallel} V_{\parallel}) \gamma^{-1}}{(\tilde{\omega}_B^2 - k_{\parallel} V_{\parallel})^2} f(p_{\parallel}, p_{\perp}) d\mathbf{p}; \quad (2.8)$$

$$\varepsilon_{33} = 1 - \int \frac{\omega_p^2}{\gamma^3 (\omega - k_{\parallel} V_{\parallel})^2} f(p_{\parallel}, p_{\perp}) d\mathbf{p}; \quad (2.9)$$

$$\varepsilon_{13} = \varepsilon_{31} = \frac{\omega_p^2}{\omega^2} \int \frac{k_{\parallel} V_{\parallel} (\omega - k_{\parallel} V_{\parallel}) \gamma^{-1}}{(\omega - k_{\parallel} V_{\parallel})^2 - \tilde{\omega}_B^2} f(p_{\parallel}, p_{\perp}) d\mathbf{p}; \quad (2.10)$$

here

$$\omega_p^2 = \frac{8\pi e^2 n_p}{m}, \quad \tilde{\omega}_B = \frac{\omega_B}{\gamma}. \quad (2.11)$$

The set of equations (2.6) splits into three equations, which correspond to three types of fundamental modes having small inclination angles with respect to the magnetic field: the transverse extraordinary X-mode (*t*-wave) with the electric field perpendicular to the $(\vec{k}\vec{B})$ plane and the longitudinal-transverse mode (*lt*_{1,2}) with the electric field in the $(\vec{k}\vec{B})$ plane with two branches: the ordinary (O) and Alfvén (A) mode. The higher frequency branch (*lt*₁) on the diagram $\omega(k)$ begins with the Langmuir frequency and for longitudinal waves ($k_{\perp} = 0$) *lt*₁ reduces to the pure longitudinal Langmuir mode (see Fig. 2.3). *lt*₁ is a superluminal wave $v_{ph} > c$ (v_{ph} is the phase velocity of the wave) and can not be excited by particles, thus, we do not consider it farther. The lower frequency branch, *lt*₂, is similar to the Alfvén wave. Analytical expressions for dispersion of these modes are available in some limits. When $k_{\perp} = 0$, the *t*-mode merges with the *lt*-modes and corresponding spectra in the laboratory frame is given by (Kazbegi et al., 1992)

$$\omega_t \approx kc(1 - \delta), \quad \delta = \frac{\omega_p^2}{4\omega_B^2 \gamma^3} \quad (2.12)$$

The resonance condition (2.3) ($s = \pm 1$) for *t*-waves with the spectrum (2.12) takes the form (Lyutikov et al., 1999b)

$$\frac{1}{2\gamma_{res}} + \frac{(k_{\perp}/k_{\varphi} - u_x/c)^2}{2} + \frac{1}{2} \frac{k_r^2}{k_{\varphi}^2} - \delta = \pm \frac{\omega_B}{\gamma_{res} k_{\varphi} c}. \quad (2.13)$$

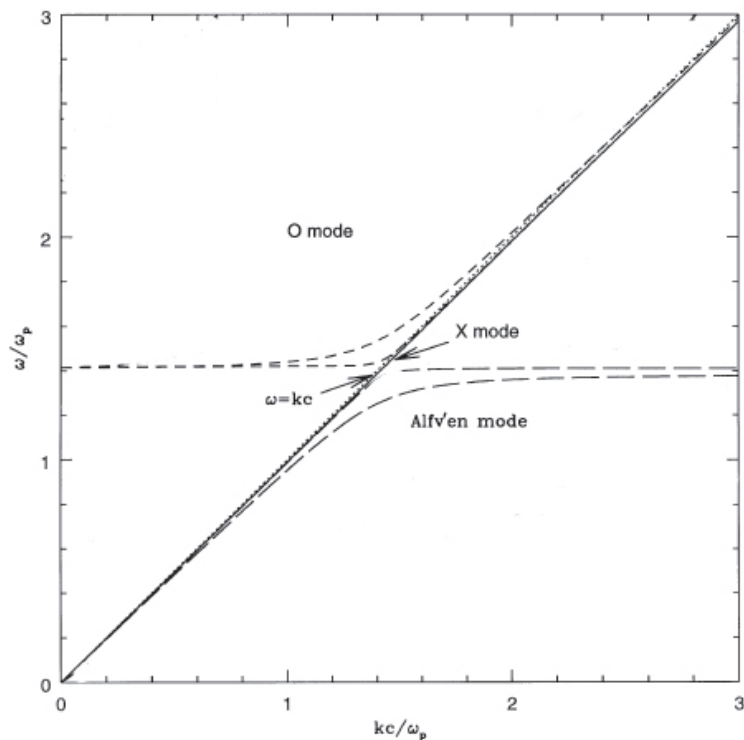


Figure 2.3: Dispersion curves for the waves in electron-positron plasma. There are three modes represented by the dashed (ordinary mode), solid (extraordinary mode) and long-dashed (Alfvén mode) lines. The dotted line represents the vacuum-dispersion relation.

From this equation we see that for wave generation by the anomalous Doppler effect (the minus sign), the following condition has to be satisfied

$$\delta > \frac{1}{2\gamma_{res}} + \frac{(k_{\perp}/k_{\varphi} - u_x/c)^2}{2} + \frac{1}{2} \frac{k_r^2}{k_{\varphi}^2}. \quad (2.14)$$

The value of δ is pretty small and the fulfilment of the condition (2.14) is quite difficult. But the relation $\omega_p^2/\omega_B^2 \sim (r/r_0)^3$ (r_0 is the pulsar radius) grows as a cube of the distance and if $\gamma_p^3 \sim 100$ (Rankin, 1983) for typical pulsar parameters the condition (2.14) is satisfied at distances $r \sim 10^9$ cm. Let us define the frequency of t -waves excited due to the cyclotron resonance. The resonance condition is easily derived for the small angles of propagation with respect to the magnetic field. Using the expression (2.12) for the dispersion of t -waves and neglecting the drift term the resonance condition (2.3) may then be written as

$$\frac{1}{2\gamma_{res}^2} - \delta + \frac{\alpha^2}{2} = -\frac{\omega_B}{\omega\gamma_{res}}. \quad (2.15)$$

First we note that Eq. (2.15) requires that $1/(2\gamma_{res}^2) < \delta$ and $\alpha^2/2 < \delta$

(here α is the angle between the wave vector and the magnetic field). First condition demonstrates that the particle is moving through the plasma with a higher velocity than the phase velocity of the wave. The second condition limits the emission to the small angles with respect to the magnetic field. For typical parameters of pulsars we have $1/(2\gamma_{res}^2) \ll \delta$ and $\alpha^2/2 \ll \delta$. Consequently, from (2.15) we find

$$\omega \approx \frac{\omega_B}{\gamma_{res}\delta}. \quad (2.16)$$

Mostly the generated waves come in the radio domain. The plus sign of Eq. (2.13) corresponds to wave damping by normal Doppler effect, which appears to be effective for smaller $\gamma_{res} \approx \gamma_p$.

So, due to the one-dimensionality of the distribution function, the radio waves are generated in the outer parts of the pulsar magnetosphere by particles with high Lorentz factors. But the particles with lower Lorentz factors cause wave damping if the resonance condition (2.3) is satisfied. Consequently, for wave generation along with the one-dimensionality of the distribution function it's also essential that it is anisotropic. The distribution function has the elongated tail in the direction of higher impulses. Thus, waves that come in the resonance with 'tail' and 'beam' electrons may be generated.

2.2 Cyclotron instability and its excitation conditions

To study the cyclotron instability in a pulsar magnetosphere we use the kinetic equation in the plasma's rest frame of the form

$$\frac{\partial f}{\partial t} + \mathbf{v} \frac{\partial f}{\partial \mathbf{r}} + \frac{\partial}{\partial \mathbf{p}} \left\{ \left(\mathbf{G} + \mathbf{F} + \mathbf{Q} + \frac{e}{c}[\mathbf{v}, \mathbf{B}_0] \right) f \right\} + e \left(\mathbf{E} + \frac{1}{c}[\mathbf{v}, \mathbf{B}] \right) \frac{\partial f}{\partial \mathbf{p}} = 0, \quad (2.17)$$

where $f(t, \mathbf{r}, \mathbf{p})$ is the particle distribution function, \mathbf{B}_0 is the magnetic field of the pulsar magnetosphere, \mathbf{E} and \mathbf{B} are the intensities of the electric and magnetic fields of induced perturbations, respectively, \mathbf{G} is the force acting on the particle and caused by inhomogeneity of the magnetic field $\mathbf{B}_0(\mathbf{r})$, \mathbf{F}

and \mathbf{Q} are the radiation deceleration forces produced by particle emission (synchrotron and curvature radiation, in particular).

The magnetic field $\mathbf{B}_0(\mathbf{r})$ is assumed to be weakly inhomogeneous - i.e.,

$$\frac{\lambda}{\mathbf{B}_0} \frac{\partial \mathbf{B}_0(\mathbf{r})}{\partial \mathbf{r}} \ll 1; \quad (2.18)$$

implying that the length of the excited waves λ is considerably less than the characteristic dimensions of the magnetic field inhomogeneity.

Dividing the distribution function into background and pulsating components

$$f = f^0 + \tilde{f}, \quad (2.19)$$

we can average (2.17) over quick pulsations. Using the method of successive approximations for a weak turbulence, when

$$\frac{|\mathbf{E}|^2}{4\pi n_p m c^2 \gamma_p} \ll 1, \quad (2.20)$$

and taking into account that $\langle f \rangle = f^0$ and $\langle \tilde{f} \rangle = 0$ (angular brackets denote averaging over pulsations) we have

$$\frac{\partial f^0}{\partial t} + \mathbf{v} \frac{\partial f^0}{\partial \mathbf{r}} + \frac{\partial}{\partial \mathbf{p}} \{ (\mathbf{G} + \mathbf{F} + \mathbf{Q}) f^0 \} = -e \left\langle \left(\mathbf{E} + \frac{1}{c} [\mathbf{v}, \mathbf{B}] \right) \frac{\partial f}{\partial \mathbf{p}} \right\rangle, \quad (2.21)$$

$$\frac{\partial \tilde{f}}{\partial t} + \mathbf{v} \frac{\partial \tilde{f}}{\partial \mathbf{r}} + \frac{\partial}{\partial \mathbf{p}} \left\{ \frac{e}{c} [\mathbf{v}, \mathbf{B}_0] \tilde{f} \right\} = -e \left(\mathbf{E} + \frac{1}{c} [\mathbf{v}, \mathbf{B}] \right) \frac{\partial f^0}{\partial \mathbf{p}}. \quad (2.22)$$

Equation (2.22) does not take into account the contribution from \mathbf{G} . For the typical pulsar parameters, it is possible if $\gamma\psi \ll 10^{10}$, which is obviously fulfilled. Note that the right-hand side of Eq. (2.21) describes diffusion of resonant particles caused by their interaction with the excited pulsations.

The plasma distribution function is one-dimensional and anisotropic (see Fig. 2.1). Thus, at a certain distance from the pulsar it may become unstable with regard to the excitation of the cyclotron oscillations on the anomalous Doppler effect ($s = +1$ in Eq. (2.3)) (Kawamura & Suzuki, 1977; Lominadze et al., 1979).

Let us consider the perturbations of such a type, propagating along the

magnetic field $\mathbf{k} \parallel \mathbf{B}_0$, with the electric vector \mathbf{E} perpendicular to \mathbf{B}_0 . Then, for each kind of particles from Eq. (2.22) we have

$$\begin{aligned} \tilde{f}(\mathbf{k}, \omega) = & -\frac{ie}{2} \left\{ \frac{(E_x - iE_y)(p_x + ip_y)}{(\omega - k_\varphi V_\varphi - k_\perp u_\perp + \omega_B/\gamma)} + \right. \\ & \left. + \frac{(E_x + iE_y)(p_x - ip_y)}{(\omega - k_\varphi V_\varphi - k_\perp u_\perp - \omega_B/\gamma)} \right\} \hat{L} f^0, \end{aligned} \quad (2.23)$$

$$\hat{L} \equiv \left(1 - \frac{k_\varphi V_\varphi}{\omega} \right) \frac{1}{p_\perp} \frac{\partial}{\partial p_\perp} + \frac{k_\varphi}{m\gamma\omega} \frac{\partial}{\partial p_\parallel}, \quad (2.24)$$

where

$$p_x = p_\perp \cos \varphi, \quad p_y = p_\perp \sin \varphi. \quad (2.25)$$

Using Eq. (2.23), one can calculate the expression for the current density and its substitution into the Maxwell's equation gives

$$1 - \frac{k^2 c^2}{\omega^2} - \sum \frac{4\pi e}{m\omega} \int \frac{f_\parallel(p_\parallel) dp_\parallel}{\gamma(\omega - k_\varphi V_\varphi - k_\perp u_\perp \mp \omega_B/\gamma)} = 0, \quad (2.26)$$

where

$$f_\parallel(p_\parallel) = \int f^0 p_\perp dp_\perp. \quad (2.27)$$

The dispersion relation (2.26) allows the following solution

$$\omega = \pm kc \left(\frac{\omega_B^2 - 2\omega_p^2}{\omega_B^2 + 2\omega_p^2} \right)^{1/2}. \quad (2.28)$$

From this expression it follows that, if the condition $2\omega_p^2 > \omega_B^2$ is fulfilled, develops a hydrodynamic hose instability, which causes 'catastrophe' - all particles take place in extraction of parallel and transversal energy. Therefore, the condition $\omega_B^2 > 2\omega_p^2$ excludes the hose instability, and under the resonance condition

$$\omega - k_\varphi V_\varphi - k_\perp u_\perp \pm \frac{\omega_B}{\gamma_{res}} = 0 \quad (2.29)$$

we obtain (Lominadze et al., 1979)

$$\text{Im } \omega \equiv \Gamma_c = \frac{\pi^2 e^2}{k_\varphi} \sum \left\{ f_\parallel \left(\frac{m\omega_B^3}{k_\varphi \omega_p^2} \right) - f_\parallel \left(\frac{m\omega_B}{k_\varphi} \right) \right\}. \quad (2.30)$$

The second term in the braces of Eq. (2.30) describes the decay of cyclotron oscillations on plasma particles and the first term corresponds to wave excitation.

2.3 The feedback of generated waves on the distribution of the resonant particles – the quasi-linear diffusion

During the generation of t or lt modes by resonant particles, one also has a simultaneous feedback of these waves on the electrons (Vedenov et al., 1961). This mechanism is described by quasi-linear diffusion (QLD), leading to the diffusion of particles as along as across the magnetic field lines. The process of the QLD in the external magnetic field is examined in a series of books (Melrose & McPhedran, 1991; Akhiezer, 1967). Generally speaking, at the pulsar surface relativistic particles efficiently lose their perpendicular momenta via synchrotron emission in very strong ($B \sim 10^{12}\text{G}$) magnetic fields and therefore, they very rapidly transit to their ground Landau state (pitch angles are vanishing). Contrary to this process, the QLD leads to the re-creation of the pitch angles by resonant particles.

Using expression (2.23) for $\tilde{f}(\mathbf{k}, \omega)$ we can obtain the right-hand side of Eq. (2.21), which describes the process of the re-distribution of the resonant particles during the development of the cyclotron instability. Assuming that $\mathbf{E} = (E_x, 0, 0)$, we will get

$$\begin{aligned} S_{QLD} &\equiv e \left\langle \left(\mathbf{E} + \frac{1}{c}[\mathbf{v}, \mathbf{B}] \right) \frac{\partial f}{\partial \mathbf{p}} \right\rangle = \\ &= \frac{\pi e^2}{2} \int d\mathbf{k} |E_k|^2 \hat{L} \frac{p_{\perp}^2}{2} \delta(\omega - k_{\parallel} V_{\parallel} + \omega_B / \gamma) \hat{L} f^0, \end{aligned} \quad (2.31)$$

where δ is the Dirac function.

Equation (2.31) describes the diffusion of particles caused by the interaction of the excited waves with the resonant particles and can be written in

the form (Lominadze et al., 1979)

$$S_{QLD} = \frac{1}{p_{\perp}} \frac{\partial}{\partial p_{\perp}} \left\{ p_{\perp} D_{\perp,\perp} \frac{\partial f^0}{\partial p_{\perp}} \right\} + \frac{1}{p_{\perp}} \frac{\partial}{\partial p_{\perp}} \left\{ p_{\perp} D_{\perp,\parallel} \frac{\partial f^0}{\partial p_{\parallel}} \right\} + \frac{\partial}{\partial p_{\parallel}} \left\{ D_{\parallel,\perp} \frac{\partial f^0}{\partial p_{\perp}} \right\} + \frac{\partial}{\partial p_{\parallel}} \left\{ D_{\parallel,\parallel} \frac{\partial f^0}{\partial p_{\parallel}} \right\}, \quad (2.32)$$

where $D_{\perp,\perp}$, $D_{\parallel,\perp}$, $D_{\perp,\parallel}$ and $D_{\parallel,\parallel}$ are the diffusion coefficients.

The wave excitation leads to a redistribution process of the particles via QLD. Using expression (2.32) we rewrite the Eq. (2.21) in the following form (Machabeli & Usov, 1979; Malov & Machabeli, 2002):

$$\begin{aligned} \frac{\partial f^0}{\partial t} + \frac{\partial}{\partial p_{\parallel}} \left\{ (G_{\parallel} + F_{\parallel} + Q_{\parallel}) f^0 \right\} + \frac{1}{p_{\perp}} \frac{\partial}{\partial p_{\perp}} \left\{ p_{\perp} (G_{\perp} + F_{\perp}) f^0 \right\} = \\ = \frac{1}{p_{\perp}} \frac{\partial}{\partial p_{\perp}} \left\{ p_{\perp} \left(D_{\perp,\perp} \frac{\partial}{\partial p_{\perp}} + D_{\perp,\parallel} \frac{\partial}{\partial p_{\parallel}} \right) f^0(\mathbf{p}) \right\} + \\ + \frac{\partial}{\partial p_{\parallel}} \left\{ \left(D_{\parallel,\perp} \frac{\partial}{\partial p_{\perp}} + D_{\parallel,\parallel} \frac{\partial}{\partial p_{\parallel}} \right) f^0(\mathbf{p}) \right\}. \end{aligned} \quad (2.33)$$

where F_{\perp} is the radiation deceleration force produced by synchrotron emission, Q_{\parallel} is the reaction force of the curvature radiation and G is the force responsible for conserving the adiabatic invariant $p_{\perp}^2/B(r) = \text{const}$. They can be written in the form (Landau & Lifshitz, 1971):

$$G_{\perp} = -\frac{c}{\rho} p_{\perp}, \quad G_{\parallel} = \frac{c p_{\perp}^2}{\rho p_{\parallel}}, \quad (2.34)$$

$$F_{\perp} = -\alpha_s \frac{p_{\perp}}{p_{\parallel}} \left(1 + \frac{p_{\perp}^2}{m^2 c^2} \right), \quad F_{\parallel} = -\frac{\alpha_s}{m^2 c^2} p_{\perp}^2, \quad (2.35)$$

$$Q_{\parallel} = -\alpha_c p_{\parallel}^4, \quad (2.36)$$

where $\alpha_s = 2e^2 \omega_B^2 / 3c^2$, $\alpha_c = 2e^2 / 3\rho^2 (mc)^4$.

The diffusion coefficients in Eq. (2.33) are evaluated in the momentum

space as (Melrose & McPhedran, 1991):

$$\begin{pmatrix} D_{\perp,\perp} \\ D_{\perp,\parallel} = D_{\parallel,\perp} \\ D_{\parallel,\parallel} \end{pmatrix} = \int \frac{d^3\mathbf{k}}{(2\pi)^3} \frac{\pi^2 e^2 v^2 \sin^2 \psi |E_k|^2}{\hbar^2 \omega^2} \frac{1}{4\pi} \times \\ \times \delta(\omega(\mathbf{k}) - k_{\parallel} v_{\parallel} + \omega_B/\gamma) \begin{pmatrix} (\Delta p_{\perp})^2 \\ (\Delta p_{\perp})(\Delta p_{\parallel}) \\ (\Delta p_{\parallel})^2 \end{pmatrix}. \quad (2.37)$$

Where $|E_k|^2/4\pi$ is the density of electric energy in the excited waves and

$$\Delta p_{\perp} = -\frac{\hbar\omega_B}{\gamma v \sin \psi}, \quad \Delta p_{\parallel} = \hbar k_{\parallel}. \quad (2.38)$$

The evaluation in our case gives (Chkheidze et al., 2010)

$$\begin{pmatrix} D_{\perp,\perp} \\ D_{\perp,\parallel} = D_{\parallel,\perp} \\ D_{\parallel,\parallel} \end{pmatrix} = \begin{pmatrix} D\delta|E_k|_{k=k_{res}}^2 \\ -D\psi|E_k|_{k=k_{res}}^2 \\ D\psi^2\frac{1}{\delta}|E_k|_{k=k_{res}}^2 \end{pmatrix}, \quad (2.39)$$

where $D = e^2/8c$.

The pitch-angle acquired by resonant particles during the process of QLD satisfies $\psi = p_{\perp}/p_{\parallel} \ll 1$. Thus, one can assume $\partial/\partial p_{\perp} \gg \partial/\partial p_{\parallel}$ which reduces Eq. (2.33) to the following form

$$\frac{\partial f^0}{\partial t} + \frac{1}{p_{\perp}} \frac{\partial}{\partial p_{\perp}} [p_{\perp}(F_{\perp} + G_{\perp})f^0] = \frac{1}{p_{\perp}} \frac{\partial}{\partial p_{\perp}} \left[p_{\perp} D_{\perp,\perp} \frac{\partial f^0}{\partial p_{\perp}} \right]. \quad (2.40)$$

Now let us compare the transverse components of the forces G and F . If we consider the case $\gamma\psi \gg 1$ we will have :

$$\frac{G_{\perp}}{F_{\perp}} = \frac{3m^3 c^6 \gamma}{2e^4 B_0^2 \rho} \left(\frac{r}{r_0} \right)^6 \frac{1}{\gamma^2 \psi^2}, \quad (2.41)$$

where r is the distance from the pulsar. For the typical parameter values of pulsars $|G_{\perp}| \ll |F_{\perp}|$.

The transversal quasi-linear diffusion increases the pitch-angle, whereas

force \mathbf{F} resists this process, leading to the stationary state ($\partial f/\partial t = 0$). Then the solution of Eq. (2.40) is

$$f(p_{\perp}) = C \exp \left(\int \frac{F_{\perp}}{D_{\perp,\perp}} dp_{\perp} \right) = C e^{-\left(\frac{p_{\perp}}{p_{\perp 0}}\right)^4}. \quad (2.42)$$

To evaluate $p_{\perp 0}$, we use the quantity $|E_k|^2 \approx mc^2 n_b \gamma_b c / (2\omega)$, where ω is the frequency of original waves, excited during the cyclotron resonance and can be estimated from expression (2.16). Consequently, we will get

$$p_{\perp 0} \approx \frac{\pi^{1/2}}{B \gamma_p^2} \left(\frac{3m^9 c^{11} \gamma_b^5}{32e^6 P^3} \right)^{1/4}. \quad (2.43)$$

As a result of the appearance of the pitch angles, the synchrotron emission is generated.

Chapter 3

Synchrotron emission

In a number of papers (Chkheidze & Machabeli, 2007; Chkheidze et al., 2010; Chkheidze, 2011), we attempted to describe the emission spectra of individual pulsars under the assumption of a synchrotron mechanism. The theory of the synchrotron emission of ultrarelativistic electrons was well developed before the discovery of pulsars. Thus, its interpretation with the high frequency radiation of pulsars did not require any farther development of the theory. In the standard theory of the synchrotron emission (Bekefi & Barrett, 1977; Ginzburg, 1981), unlike the present model, it is supposed that the observed radiation is collected from a large spacial region in various parts of which, the magnetic field is oriented randomly. Thus, it is supposed that along the line of sight the magnetic field directions are chaotic leading to the broad interval (from 0 to π) of the pitch angles. According to our model the emission comes from a region of the pulsar magnetosphere where the magnetic field lines are practically straight and parallel to each other. Contrary to the standard scenario, as we have already outlined, in the pulsar magnetospheres the magnetic field is very strong and pitch angles rapidly vanish. The present model provides all necessary conditions for re-creation of the pitch angles, and as we take into account the mechanism of creation of the pitch angles, their possible values are inevitably restricted.

3.1 Synchrotron radiation of a single electron

Synchrotron emission is a type of radiation generated by charged particles spiralling around magnetic field lines at close to the speed of light. The spiral motion of the electron along the uniform magnetic field line can be split into motion along the magnetic field direction with the constant velocity $v_{\parallel} = v \cos \psi$ and circular motion with the velocity $v_{\perp} = v \sin \psi$ and radius $r_B = cmv_{\perp}\gamma/eB$ about it. The angular frequency of the electron in its orbit is $\tilde{\omega}_B = \omega_B/\gamma$. Synchrotron emission of a single electron is strongly beamed along the direction of motion in a cone of approximate opening half-angle $\sim 1/\gamma$. Therefore, the observer detects the significant radiation when the angle between the observer's axis and \vec{v} is less than $1/\gamma$. When the pitch-angle of the particle $\psi > 1/\gamma$ the observer receives emission impulses with the width Δt that are separated by time interval T . The quantity T is defined by the angular frequency of the electron and Doppler's effect (Ginzburg, 1981)

$$T = \frac{2\pi}{\tilde{\omega}_B} \left(1 - \frac{v_{\parallel} \cos \psi}{c} \right). \quad (3.1)$$

The duration of the emission impulse

$$\Delta t \approx \frac{mc}{eB_{\perp}} \frac{1}{\gamma^2}, \quad (3.2)$$

where $B_{\perp} = B \sin \psi$. The synchrotron spectrum consists of the harmonics with the fundamental frequency

$$\omega_0 = \frac{2\pi}{T} = \frac{eB}{mc\gamma} \frac{1}{1 - (v_{\parallel}/c) \cos \psi}. \quad (3.3)$$

And the maximum of the emission spectrum comes on frequency

$$\omega_m \simeq \frac{1}{\Delta t} \approx \frac{eB_{\perp}\gamma^2}{mc}. \quad (3.4)$$

As for ultrarelativistic particles $\omega_m \gg \omega_0$, the synchrotron emission is assumed as continuous radiation. Thus, one can introduce the spectral flux

density of the synchrotron emission of a single electron as

$$\tilde{p}_\nu^* = \frac{3}{4\pi^2 r^2} \frac{e^3 B}{mc^2 \xi} \left(\frac{\nu}{\nu_c} \right)^2 \left(1 + \frac{\chi^2}{\xi^2} \right) \left[K_{2/3}^2(g_\nu) + \frac{\chi^2}{\xi^2} K_{1/3}^2(g_\nu) \right], \quad (3.5)$$

where $\xi = 1/\gamma$, χ is the angle between \vec{v} and the observer's axis,

$$g_\nu = \frac{\nu}{2\nu_c} \left(1 + \frac{\psi^2}{\xi^2} \right)^{3/2}, \quad (3.6)$$

$$\nu_c = \frac{3eB_\perp}{4\pi mc} \gamma^2, \quad (3.7)$$

r is the distance between the observer and the emitting particle, $K_{1/3}$ and $K_{2/3}$ are the Macdonald functions (Ginzburg, 1981).

Now let us find the spectral distribution of the synchrotron radiation of a single electron p_ν^* . For this reason one should integrate the expression (3.5) over a closed surface around the emitting particle. The quantity \tilde{p}_ν^* tends rapidly to zero when $\chi > \xi$. Thus, when integrating it over the closed surface the significant contribution brings in only the annular sector $\Delta\Omega = 2\pi \sin\psi \Delta\chi$. Consequently we can write

$$p_\nu^* = 2\pi r^2 \sin\psi \int_{-\infty}^{+\infty} \tilde{p}_\nu^* d\chi. \quad (3.8)$$

The integral (3.8) can be rewritten as (Ginzburg, 1981)

$$p_\nu^* = \frac{\sqrt{3}e^3 B_\perp}{mc^2 \sin^2\psi} \frac{\nu}{\nu_c} \int_{\nu/\nu_c}^{\infty} K_{5/3}(z) dz. \quad (3.9)$$

The observed spectral flux density \tilde{p}_ν^* is not equal to emitted spectral power density p_ν . The reason for this is the finite speed of propagation of radiated photons. In particular, the photons emitted during the time period dt' will be detected by observer during the time period $dt = dt'(1 - v_r/c)$, where v_r is the electron's velocity projection on the observer's direction. In our case $v_r = v \cos^2\psi$. Consequently we will have

$$p_\nu = p_\nu^* \left(1 - \frac{v}{c} \cos^2\psi \right) \approx p_\nu^* \sin^2\psi = \frac{\sqrt{3}e^3 B_\perp}{mc^2} \frac{\nu}{\nu_c} \int_{\nu/\nu_c}^{\infty} K_{5/3}(z) dz. \quad (3.10)$$

The maximum of synchrotron spectrum of a single electron comes on frequency

$$\nu_m = 0.29\nu_c = 0.07 \frac{eB_\perp}{mc} \gamma^2 \approx 1.2 \cdot 10^6 B_\perp \gamma^2 \text{Hz}. \quad (3.11)$$

The synchrotron emission power density can be approximately expressed for lower ($\nu \ll \nu_m$) and higher ($\nu \gg \nu_m$) frequencies in the following form

$$p_\nu \simeq \frac{\sqrt{3}e^3 B_\perp}{mc^2} \times \begin{pmatrix} 2^{2/3} \Gamma\left(\frac{2}{3}\right) \left(\frac{\nu}{\nu_c}\right)^{1/3}, & \text{if } \nu \ll \nu_m \\ \sqrt{\frac{\pi}{2}} \frac{\nu}{\nu_c} \exp\left(-\frac{\nu}{\nu_c}\right), & \text{if } \nu \gg \nu_m \end{pmatrix}. \quad (3.12)$$

Here $\Gamma(2/3)$ - is a Gamma function.

If we integrate p_ν over the frequency, we will get the expression for the energy loss rate of the emitting particle

$$-\frac{d\varepsilon_e}{dt} = \frac{2}{3} c \left(\frac{e^2}{mc^2}\right)^2 B_\perp^2 \left(\frac{\varepsilon_e}{mc^2}\right)^2, \quad (3.13)$$

where ε_e is the energy of the electron. The characteristic time of energy loss by relativistic electron via synchrotron emission is

$$\tau \equiv \frac{\varepsilon_e}{d\varepsilon_e/dt} = \frac{5.1 \cdot 10^8}{B_\perp^2 (\varepsilon_e/mc^2)} \text{ s}. \quad (3.14)$$

3.2 Synchrotron spectrum of the set of electrons

3.2.1 The standard approach

Let us consider the synchrotron emission of the set of electrons. If the set of emitting particles is stationary or changes quite slowly, one should use quantity $\tilde{p}_\nu = \tilde{p}_\nu^* \sin^2 \psi$ in place of \tilde{p}_ν^* . The number of emitting particles in the elementary dV volume is $f d\varepsilon dV d\Omega_\tau$, with the energy from the interval $\varepsilon, \varepsilon + d\varepsilon$ and with velocities that lie inside the solid angle $d\Omega_\tau$ near the direction of $\vec{\tau}$ (here f is the distribution function of the emitting particles). If the emission of individual electrons is incoherent, then \tilde{p}_ν is the additive

quantity and the emission flux of the set of electrons will be (Ginzburg, 1981)

$$F_\nu = \int \tilde{p}_\nu f d\varepsilon dV d\Omega_\tau. \quad (3.15)$$

The integration over $d\Omega_\tau$ in this case can be done in the general form. In particular, the integrand is nonzero only in a small angular interval $\Delta\chi \sim 1/\gamma$. Thus, when integrating (3.15) over $d\Omega_\tau$ the significant contribution is only brought in by the narrow annular sector $\Delta\Omega_\tau = 2\pi \sin\alpha \Delta\chi$, where $\alpha = \psi - \chi \approx \psi$ - is the angle between the magnetic field and the observer's direction. Consequently, one can extend the integration over χ to the entire band from $-\infty$ to $+\infty$. Taking into account the Eqs. (3.8) and (3.9), in place of (3.15) we will get

$$F_\nu = \frac{\sqrt{3}e^3}{mc^2} \int f(\varepsilon) B \sin\psi \left(\frac{\nu}{\nu_c}\right) \left[\int_{\nu/\nu_c}^{\infty} K_{5/3}(z) dz \right] d\varepsilon \quad (3.16)$$

Let us consider the synchrotron emission of the set of electrons with a power-law energy distribution

$$f \propto \varepsilon^{-a}, \quad \varepsilon_{\min} \leq \varepsilon \leq \varepsilon_{\max} \quad (\varepsilon_{\max} \gg \varepsilon_{\min}). \quad (3.17)$$

If we change the integration variable ε by $x = \nu/\nu_c$ the integral (3.16) will take the form

$$F_\nu = \frac{\sqrt{3}e^3}{2mc^2} \left(\frac{3e}{4\pi m^3 c^5}\right)^{1/2(a-1)} (B \sin\psi)^{1/2(a+1)} \nu^{-1/2(a-1)} \times \\ \times \left[G\left(\frac{\nu}{\nu_c}\right)_{\max} - G\left(\frac{\nu}{\nu_c}\right)_{\min} \right], \quad (3.18)$$

where

$$G(y) = \int_y^\infty x^{1/2(a-1)} \int_x^\infty K_{5/3}(z) dz dx. \quad (3.19)$$

It is obvious that choosing the various values for a , ε_{\max} and ε_{\min} we can obtain various spectral distributions. But if the values of ε_{\max} and ε_{\min} are such that, in the given frequency domain the conditions $(\nu/\nu_c)_{\max} \ll 1$ and

$(\nu/\nu_c)_{\min} \gg 1$ are fulfilled, the integral (3.19) is close to $G(0)$

$$G(0) = 2^{1/2(a-3)} \frac{a + \frac{7}{3}}{a + 1} \Gamma\left(\frac{3a - 1}{12}\right) \Gamma\left(\frac{3a + 7}{12}\right). \quad (3.20)$$

Consequently, we will have

$$F_\nu \propto (B \sin \psi)^{1/2(a+1)} \nu^{-1/2(a-1)}. \quad (3.21)$$

In the standard theory of the synchrotron emission (Ginzburg, 1981), it is supposed that the observed radiation is collected from a large spacial region in various parts of which, the magnetic field is oriented randomly. Thus, it is supposed that along the line of sight the magnetic field directions are chaotic. Hence, to find the emission flux, we need to average Eq. (3.21) over all directions of the magnetic field (which means integration over ψ varying from 0 to π). Taking into account, that

$$1/2 \int_0^\pi (\sin \psi)^{1/2(a+1)} \sin \psi d\psi = \frac{\sqrt{\pi} \Gamma(1/4(a + 5))}{2 \Gamma(1/4(a + 7))}. \quad (3.22)$$

We can write

$$F_\nu \propto \nu^{-\beta}, \quad \beta = 1/2(a - 1). \quad (3.23)$$

This is a power-law synchrotron emission flux of the set of electrons with the homogeneous and isotropic energy distribution (3.17) in the chaotic magnetic field.

3.2.2 The model

Contrary to the standard scenario, we take into account the mechanism of creation of the pitch angles. As we have already outlined in the previous chapter, at the pulsar surface the magnetic field is very strong and pitch angles rapidly vanish. The present model provides all necessary conditions for re-creation of the pitch angles on the light cylinder length-scales (the region of the pulsar magnetosphere near the light cylinder where the magnetic field lines are practically straight and parallel to each other). We obtain a certain distribution function of the emitting particles from their perpendicular mo-

menta (see Eq. (2.42)), consequently restricting their values. Synchrotron emission is generated as a result of the appearance of pitch angles.

Let us find the spectral distribution of synchrotron emission of the set of electrons in the framework of the present model. The number of emitting particles in the elementary dV volume is $p_{\perp} f dp_{\perp} dp_{\parallel} dV d\Omega_{\tau}$, with momenta from the intervals $[p_{\perp}, p_{\perp} + dp_{\perp}]$ and $[p_{\parallel}, p_{\parallel} + dp_{\parallel}]$, and with the velocities that lie inside the solid angle $d\Omega_{\tau}$ near the direction of $\vec{\tau}$. If we write the parallel distribution function of the emitting particles as $\int p_{\perp} f dp_{\perp} \equiv f_{\parallel}(p_{\parallel})$, then the emission flux of the set of electrons will be

$$F_{\nu} = \int \tilde{p}_{\nu} f_{\parallel}(p_{\parallel}) dp_{\parallel} dV d\Omega_{\tau}, \quad (3.24)$$

here \tilde{p}_{ν} is the additive quantity, as the observed synchrotron radiation wavelength λ is much less than the value of $n^{-1/3}$ - the average distance between particles, where n is the density of plasma component electrons. After integrating Eq. (3.24) over $d\Omega_{\tau}$ as in previous case and using the expression (3.9), the integral (3.24) takes the form

$$F_{\epsilon} \propto \int f_{\parallel}(p_{\parallel}) B \psi \frac{\epsilon}{\epsilon_m} \left[\int_{\epsilon/\epsilon_c}^{\infty} K_{5/3}(z) dz \right] dp_{\parallel} \quad (3.25)$$

(we changed ν by photon energy $\epsilon = h\nu$, here h is the Planck constant). If we substitute the mean value of the pitch-angle from Eq. (2.43) in the expression for $\epsilon_c \approx 5 \cdot 10^{-12} B \psi \gamma^2 \text{keV}$, we will have

$$\epsilon_c \simeq 5 \cdot 10^{-12} \frac{\pi^{1/2}}{\gamma_p^2} \left(\frac{3m^5 c^7 \gamma_b^9}{32e^6 P^3} \right)^{1/4} \quad (3.26)$$

To find the synchrotron flux in our case, we need to know the one-dimensional distribution function of the emitting particles f_{\parallel} . Let us multiply both sides of Eq. (2.33) on p_{\perp} and integrate it over p_{\perp} . Using Eqs. (2.34), (2.35), (2.36) and also taking into account that the distribution function vanishes at the boundaries of integration, Eq. (2.33) reduces to

$$\frac{\partial f_{\parallel}}{\partial t} = \frac{\partial}{\partial p_{\parallel}} \left[\left(\frac{\alpha_s}{m^2 c^2 \pi^{1/2}} p_{\perp 0}^2 + \alpha_c \gamma^4 - \frac{e^2}{4mc^2 \gamma} |E_k|^2 \right) f_{\parallel} \right]. \quad (3.27)$$

Let us estimate the contribution of different terms on the righthand side of Eq. (3.27). The estimations show that for the typical parameters of pulsars, the first term is much bigger than the two other terms. Consequently, instead of Eq. (3.27), one gets

$$\frac{\partial f_{\parallel}}{\partial t} = \frac{\partial}{\partial p_{\parallel}} \left(\frac{\alpha_s}{m^2 c^2 \pi^{1/2}} p_{\perp 0}^2 f_{\parallel} \right). \quad (3.28)$$

Considering the quasi-stationary case we find

$$f_{\parallel} \propto \frac{1}{p_{\parallel}^{1/2} |E_k|}. \quad (3.29)$$

For $\gamma\psi \ll 10^{10}$, a magnetic field inhomogeneity does not affect the process of wave excitation. The equation that describes the cyclotron noise level, in this case, has the form (Lominadze et al., 1983)

$$\frac{\partial |E_k|^2}{\partial t} = 2\Gamma_c |E_k|^2 f_{\parallel}, \quad (3.30)$$

where

$$\Gamma_c = \frac{\pi^2 e^2}{k_{\parallel}} f_{\parallel}(p_{res}), \quad (3.31)$$

is the growth rate of the instability and is defined from Eq. (2.30). Here k_{\parallel} can be found from expression (2.16) for the frequency of the excited waves

$$k_{\parallel res} \approx \frac{\omega_B}{c\delta\gamma_{res}}. \quad (3.32)$$

Combining Eqs. (3.28) and (3.30) one finds

$$\frac{\partial}{\partial t} \left\{ f_{\parallel} - \alpha \frac{\partial}{\partial p_{\parallel}} \left(\frac{|E_k|}{p_{\parallel}^{1/2}} \right) \right\} = 0, \quad (3.33)$$

$$\alpha \equiv \left(\frac{4}{3} \frac{e^2}{\pi^5 c^5} \frac{\omega_B^6 \gamma_p^3}{\omega_p^2} \right)^{1/4}, \quad (3.34)$$

which reduces to

$$\left\{ f_{\parallel} - \alpha \frac{\partial}{\partial p_{\parallel}} \left(\frac{|E_k|}{p_{\parallel}^{1/2}} \right) \right\} = \text{const.} \quad (3.35)$$

Taking into account that for the initial moment the major contribution of the lefthand side of the Eq. (3.35) comes from $f_{\parallel 0}$, the corresponding expression writes as

$$f_{\parallel} - \alpha \frac{\partial}{\partial p_{\parallel}} \left(\frac{|E_k|}{p_{\parallel}^{1/2}} \right) = f_{\parallel 0}. \quad (3.36)$$

The distribution function f is proportional to $n \sim 1/r^3$, then one should neglect f_{\parallel} in comparison with $f_{\parallel 0}$. Consequently, the above equation reduces to

$$\alpha \frac{\partial}{\partial p_{\parallel}} \left(\frac{|E_k|}{p_{\parallel}^{1/2}} \right) + f_{\parallel 0} = 0. \quad (3.37)$$

As we can see the function $E_k(p_{\parallel})$ drastically depends on the form of the initial distribution of the resonant electrons. According to the work, (Goldreich & Julian, 1969), a spinning magnetized NS generates an electric field which extracts electrons from the star's surface and accelerates them to form a low-density ($n_b = B/Pce$) and energetic primary beam. We only know the scenario of creation of the primary beam, but nothing can be told about its distribution, which drastically depends on the NS surface properties and temperature. To our knowledge there is no convincing theory which could predict the form of the distribution function of the beam electrons. Thus, we can only assume that the beam electrons have a power-law distribution

$$f_{\parallel 0} \propto p_{\parallel}^{-n}, \quad (3.38)$$

and for the energy density of the waves we get

$$|E_k|^2 \propto p_{\parallel}^{3-2n}. \quad (3.39)$$

The effective value of the pitch angle depends on $|E_k|^2$ as follows

$$\psi_0 = \frac{1}{2\omega_B} \left(\frac{3m^2 c^3 \omega_p^2}{p_{\parallel}^3 \gamma_p^3} |E_k|^2 \right)^{1/4}. \quad (3.40)$$

Using expression (3.29), (3.39) and (3.40), and replacing the integration variable p_{\parallel} by $x = \epsilon/\epsilon_m$, from Eq. (3.25) we will get (Chkheidze et al., 2010)

$$F_{\epsilon} \propto \epsilon^{-\frac{2-n}{4-n}} \int x^{\frac{2-n}{4-n}} \left[\int_x^{\infty} K_{5/3}(z) dz \right] dx. \quad (3.41)$$

The integral (3.41) can be approximately expressed by two different types of functions, depending on the values of ϵ_{\max} , ϵ_{\min} , $p_{\parallel\max}$ and $p_{\parallel\min}$

$$F_{\epsilon} \propto \left\{ \begin{array}{l} \epsilon^{-\mu} \\ \epsilon^{-\mu} \exp(-\epsilon^{\eta}) \end{array} \right\}, \quad (3.42)$$

where $\eta > 0$ and μ takes as positive, also the negative values. Consequently, we conclude that the observed synchrotron spectrum of the set of electrons with the power-law distribution function might be: the power-law, or the power-law with an exponential cutoff.

Chapter 4

RX J1856.5-3754 and RX J2143.0+0654 (RBS1774)

RX J1856.5-3754 (hereafter RXJ1856) is one of the brightest nearby isolated neutron stars, and considerable observational resources have been devoted to it. RXJ1856 was discovered by ROSAT as an X-ray source (Walter et al., 1996). According to the observational evidence, the emission of RXJ1856 did not show any significant periodic variations, and the featureless X-ray spectrum was best fitted by the Planckian spectrum with a temperature $kT_{bb}^{\infty} \simeq 63 \pm 3\text{eV}$ (Burwitz et al., 2003). Thus, it has been proposed that the emission of this source has a thermal nature and every effort directed to making a model which would describe the overall spectra well.

Walter & Mattews (1997) and Neuhäuser & Walter (1998) found an optical counterpart for RXJ1856 with $V = 26\text{mag}$. This and the large proper motion of $\simeq 0.33\text{mas yr}^{-1}$ (Walter, 2001; Neuhäuser, 2001) are additional arguments that it is indeed an isolated NS. Walter (2001) also detected parallactic motion, determined the distance to the source $d = 61_{-8}^{+9}\text{pc}$ and suggested that RXJ1856 could be the remnant of the original primary of ζ Oph the system. This implies a NS age of $\sim 10^6\text{yr}$.

First spectral modeling of RXJ1856 has been presented by (Pavlov et al., 1996). It is shown that the light element (hydrogen or helium) nonmagnetic NS atmosphere models can be firmly ruled out, because they overpredict

the optical flux by a large factor. On the other hand, no acceptable fit can be obtained with iron and standard solar-mixture atmosphere models, because the features predicted by these models are not detected with high significance. Doppler smearing of the spectral lines due to fast rotation of an NS does not completely wash away the strongest spectral features (Pavlov, Zavlin & Sanwal, 2002; Braje & Romani, 2002). Similar problems occur for highly magnetized NS atmosphere models (Rajagopal et al., 1997; Zavlin et al., 2002), so one has to conclude that the classic NS atmosphere models are unable to explain the observed X-ray emission of RXJ1856.

Different explanations have been considered (e.g., Burwitz et al. (2001); Turolla, Zane & Drake (2004)). It has been proposed that the star has no atmosphere but a condensed matter surface. The mentioned surface might result in a virtually featureless Planckian spectrum in the soft X-ray band. Yet another problem arose from the fact that the parameters derived from X-rays do not fit the optical spectrum with an intensity 6 times higher than that of X-ray emission. This situation led Pons et al. (2002) to introduce the overall spectra by two components. In this model the soft-component of $kT_{bb}^\infty \simeq 20\text{eV}$ represents radiation from a relatively cool surface and fit the optical data, when the hard component of $kT_{bb}^\infty \simeq 55\text{eV}$ emitted from $\sim 20\%$ of the NS surface is responsible for the X-ray emission.

The current thermal emission models are unable to satisfactorily explain the data. The most adequate fits of the spectra give models which assume that the star has a thin, magnetic, partially ionized hydrogen atmosphere superposed on a condensed matter surface (Motch et al., 2003; Ho et al., 2007). However, the origin of such thin hydrogen layers fitting the data is a problematic issue.

RBS1774 (1RXS J214303.7+065419) has been the most recent XDINS to be found (Zampieri et al., 2001). Its X-ray spectrum is well reproduced by an absorbed blackbody with a temperature $kT \sim 100\text{eV}$ and with a total column density of $n_H \sim 3 \cdot 10^{20} \text{cm}^{-2}$. Application of more sophisticated, and physically motivated models for the surface emission (atmospheric models) result in worse agreement with the data (Zane et al., 2005). According to

Schwope et al. (2009), a fit to the X-ray spectra extracted from RGS spectrographs onboard XMM-Newton yields that the best result is obtained when the two-temperature blackbody model is used. But the same model applied to the X-ray spectra extracted from three EPIC detectors does not improve the fit compared to the simple blackbody model.

Zane et al. (2008) revealed a spectral feature at ~ 0.7 keV. The most likely interpretation is that it is due to proton cyclotron resonance, which implies ultrastrong magnetic field of $B_{cyc} \sim 10^{14}$ G (Zane et al., 2005; Rea et al., 2007). Although, the required strong magnetic field is inconsistent with timing measurements giving $B_{dip} = 3.2 \cdot 10^{19} \sqrt{P\dot{P}} \simeq 2 \cdot 10^{13}$ G (Kaplan & van Kerkwijk, 2009).

One of the XDINS which so far eluded optical identification is RBS1774. Zane et al. (2008) reported the first detection of a likely optical counterpart for RBS1774. Standardly, optical identifications of isolated neutron stars are robustly confirmed either by the detection of optical pulsations or by the measurement of a significant proper motion. In absence of such information one can base the optical identification only on the positional coincidence between the coordinates of the candidate counterpart and those of RBS1774, as measured in the X-rays.

To make these models work, it has been postulated that the star has a condensed-matter surface. However, condensation of surface matter requires very specific conditions to be fulfilled (Lai & Salpeter, 1997; Lai, 2001). Even if these conditions are satisfied, the formation of a non-uniform distribution of the surface temperature is more likely artificial and needs to be examined by convincing theory.

In the present chapter we explain the observed X-ray spectra of two 'XDINS' (RX J1856.5-3754 and RBS1774) based on our plasma emission model (Chkheidze & Machabeli, 2007; Chkheidze, 2011). This model suggests that the emission from these object is generated by a synchrotron mechanism, switched on as the result of acquirement of pitch angles by relativistic electrons during the quasi-linear stage of the cyclotron instability. The model gives successful fits for broadband spectra, without facing problems typical

of the thermal radiation models. Considering the case of a nearly aligned rotator, it was predicted that the source should have pulsed with a period $P \sim 1$ s (Chkheidze & Machabeli, 2007). However, subsequent XMM-Newton observations of RXJ1856 discovered that its X-ray emission pulsates with a period $P_{obs} = 7.055$ s (Tiengo & Mereghetti, 2007). This has been explained in the framework of the drift wave driven model (Chkheidze & Lomiashvili, 2008). In particular, the real spin period of the pulsar might differ from the observable one, as a consequence of the existence of very low frequency drift waves in the region of generation of the pulsar emission. These waves are not directly observable but result in a periodic change of curvature of the magnetic field lines and, hence, a periodic change of the emission direction with a period of the drift waves assumed to be equal to the observable period (Lomiashvili et al., 2006).

4.1 X-ray spectral analysis

For the primary beam electrons with the Lorentz factor $\gamma_b \sim 10^7$ the emitted photon energy $\epsilon_c \sim 0.1$ keV (Eq. (3.26)) comes in the energy domain of the observed X-ray emission of RXJ1856 and RBS1774. Thus, we suppose that the measured X-ray spectrum is the result of the synchrotron emission of primary beam electrons (the resonance occurs on the right slope of the distribution function of beam electrons (see Fig. 2.1)), switched on as the result of acquirement of pitch angles by particles during the quasi-linear stage of the cyclotron instability.

Here we assume that the initial energy distribution in the beam has a Gaussian shape

$$f_{b0} = \frac{n_b}{\sqrt{\pi}\gamma_T} \exp \left[-\frac{(\gamma - \gamma_b)^2}{\gamma_T^2} \right], \quad (4.1)$$

where $\gamma_T \simeq 10$ - is the half width of the distribution function and n_b is the density of primary beam electrons. Since $\gamma_T \ll \gamma_b$, this distribution is very close to δ -function. Consequently, the electron distribution can be taken as monoenergetic.

In this case from Eq. (3.37) we get the following expression for the energy density of the waves

$$|E_k|^2 \propto p_{\parallel}. \quad (4.2)$$

Using expressions (3.29), (3.40) and (4.2) in place of integral (3.41) we will get

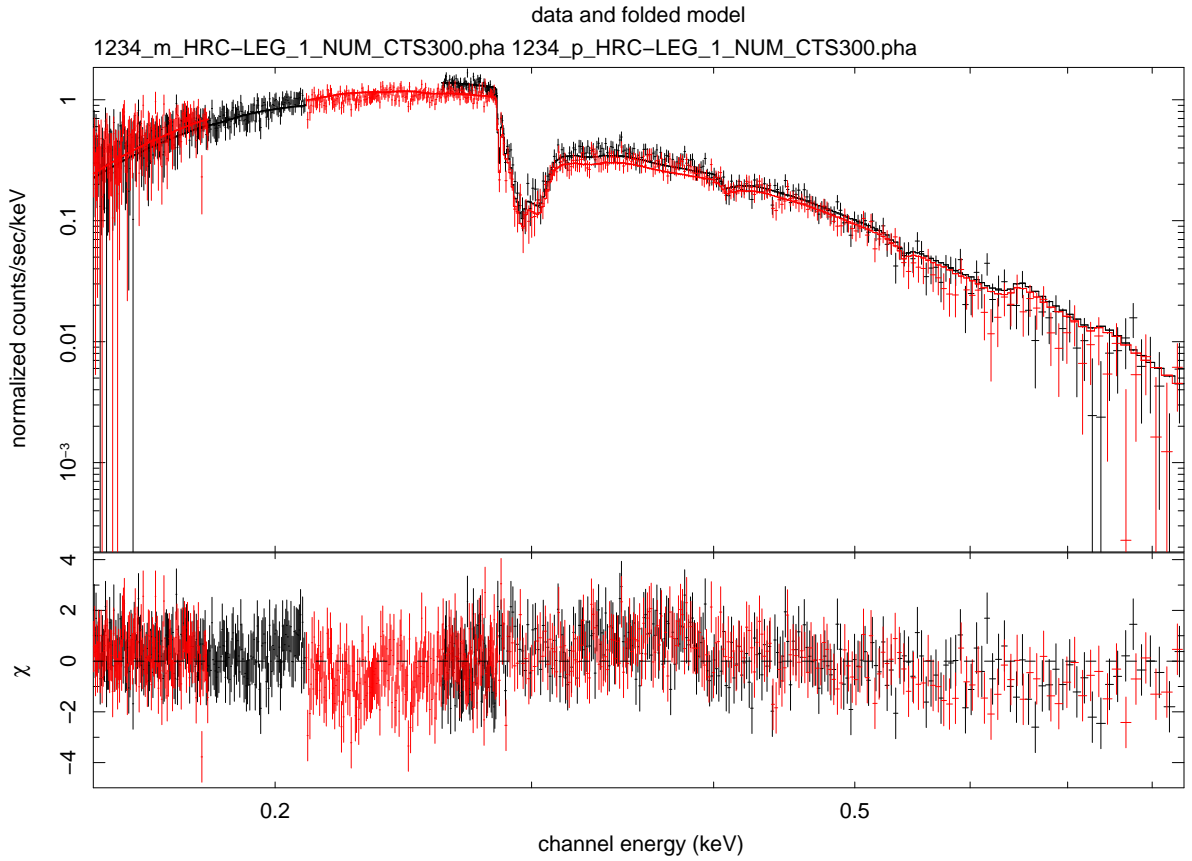
$$F_{\epsilon} \propto \epsilon^{-0.3} \int x^{0.3} \left[\int_x^{\infty} K_{5/3}(z) dz \right] dx. \quad (4.3)$$

The energy of the beam electrons vary in a small interval ($\gamma_T \ll \gamma_b \sim 10$). In this case the integral (4.3) can be approximately expressed by the following function

$$F_{\epsilon} \propto \epsilon^{0.3} \exp(-\epsilon/\epsilon_m). \quad (4.4)$$

A spectral analysis was performed with XSPEC V12.3.0. We used the model spectrum (Eq. (4.4)) absorbed by cold interstellar matter for fitting the data. The observed X-ray spectrum of RXJ1856 was extracted from CHANDRA LETGS instrument and the spectral analysis was limited to energies between 0.15 and 0.85 keV. The resulting $\chi^2 = 1.00$ for 970 degrees of freedom and the amount of interstellar matter $n_H = (1.20 \pm 0.03) \times 10^{20} \text{cm}^{-2}$ (see Fig. 4.1). The fitting results are listed in Table 4.1.

For RBS1774 we performed the spectral analysis by fitting the combined data extracted of the three EPIC X-ray cameras of the XMM-Newton Telescope (the spectral analysis was limited to energies between 0.2 and 1.5 keV). The resulting $\chi^2 = 1.63$ for 311 degrees of freedom and the amount of interstellar matter $n_H = (3.36 \pm 0.2) \times 10^{20} \text{cm}^{-2}$, which appears to be close to the total Galactic absorption in the source direction ($n_H = 5 \cdot 10^{20} \text{cm}^{-2}$ Dickey & Lockman (1990)). The spectral feature at $\sim 0.7 \text{keV}$ that is mostly described as an absorption edge or line (Zane et al., 2005; Schwobe et al., 2009) is also evident in our case from inspection of Fig. 4.2.



1-Dec-2010 20:03

Figure 4.1: The Chandra LETGS X-ray spectrum of RXJ1856, fitted with the model.

Table 4.1: The model parameters of RXJ1856 for fit to Chandra LETGS spectrum in the energy interval 0.15 – 0.85 keV. (The fitting results with a pure blackbody model absorbed by cold interstellar matter are from Burwitz et al. (2003))

Model	n_H (10^{20} cm^{-2})	ϵ_m^{-1} (eV)	kT_{bb}^∞	$\chi^2(\text{dof})$
plasma	$1.20^{+0.03}_{-0.03}$	11.54 ± 0.78		1.00(970)
bbody	$0.95^{+0.03}_{-0.03}$		63.5 ± 0.2	1.20(1145)

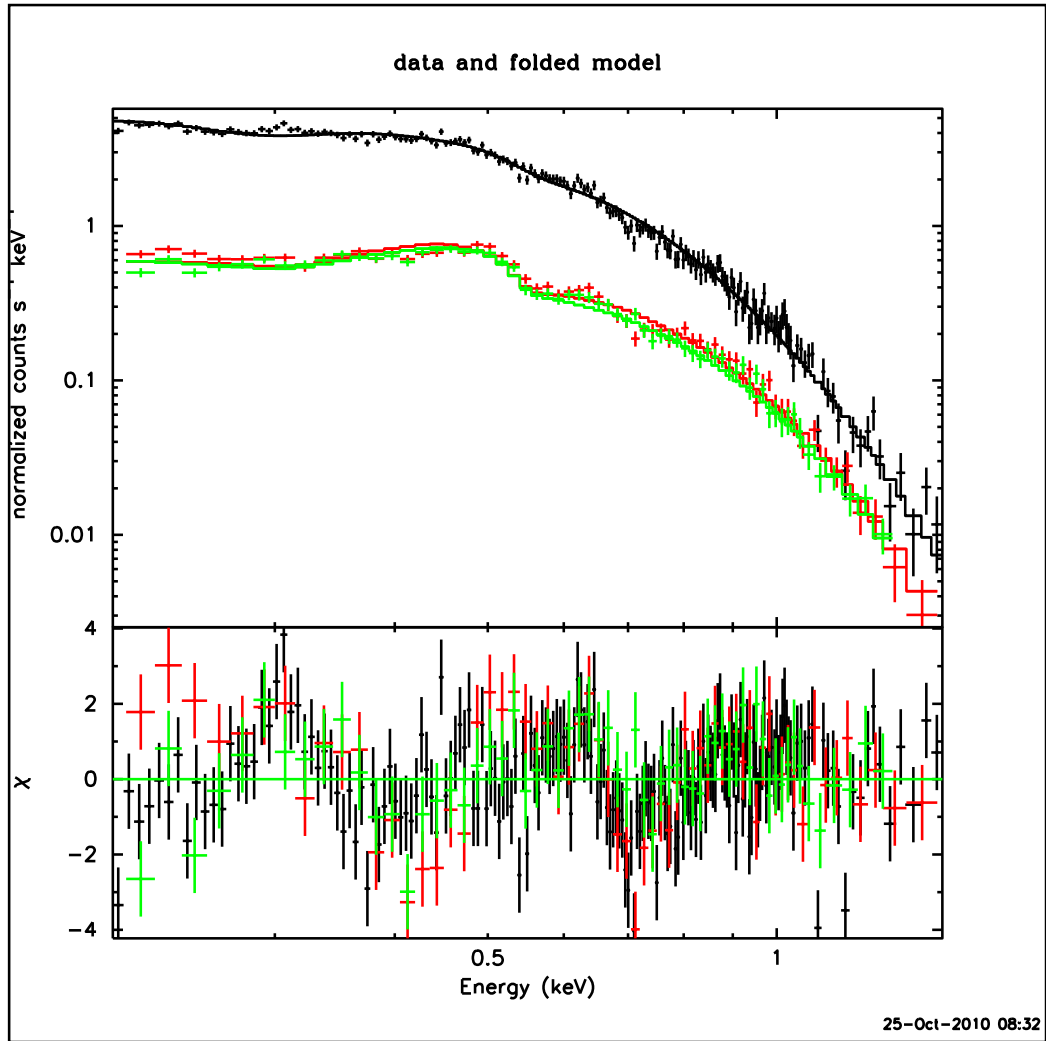


Figure 4.2: EPIC-pn and EPIC-MOS spectra of RBS1774, fitted with a model.

4.2 Possible nature of the spectral feature in the X-ray emission of RBS1774

During the farther motion in the pulsar magnetosphere, the X-ray emission of RBS1774 that is generated on the light cylinder lengthscales, might come in the cyclotron damping range (Khechinashvili & Melikidze, 1997):

$$\omega - k_{\parallel} V_{\parallel} - k_x u_x - \frac{\omega_B}{\gamma_r} = 0. \quad (4.5)$$

The condition for the development of the cyclotron instability may be easily derived for the small angles of propagation with respect to the magnetic field. Representing the dispersion of the waves as

$$\omega = kc, \quad (4.6)$$

and neglecting the drift term, the resonance condition (4.5) may then be written as

$$\frac{1}{2\gamma_r^2} + \frac{\alpha^2}{2} = \frac{\omega_B}{\omega\gamma_r}, \quad (4.7)$$

where $\alpha \approx \psi$ is the angle between the wave vector and the magnetic field. Taking into account that $\psi_0^2 \gg 1/2\gamma_b^2$ one finds from Eq. (4.7) the frequency of damped waves

$$\omega_d \approx \frac{2\omega_B}{\gamma_r\psi^2}. \quad (4.8)$$

If we assume that damping happens on the left slope of the distribution function of primary beam electrons (see Fig. 2.1), then the estimation shows that on the light cylinder lengthscales the photon energy of damped waves will be $\epsilon_d = (h/2\pi)\omega_d \simeq 0.7\text{keV}$. Taking into account the shape of the distribution function of beam electrons, we interpret the large residuals around $\sim 0.7\text{keV}$ (see Fig. 4.2) as an absorption edge. Including an absorption edge improves the fit leading to a reduced $\chi^2 = 1.50$ (for 309 degrees of freedom). The best-fitting energy of the edge is $E_{edge} = 0.679 \pm 0.013\text{keV}$, and the optical depth is $\tau_{edge} = 0.20 \pm 0.03$ (see parameters in Tab. 4.2). However, adding an absorption edge to the model spectrum does not produce a statistically significant improvement of the fitting (see Fig. 4.3). According to Schwöpe

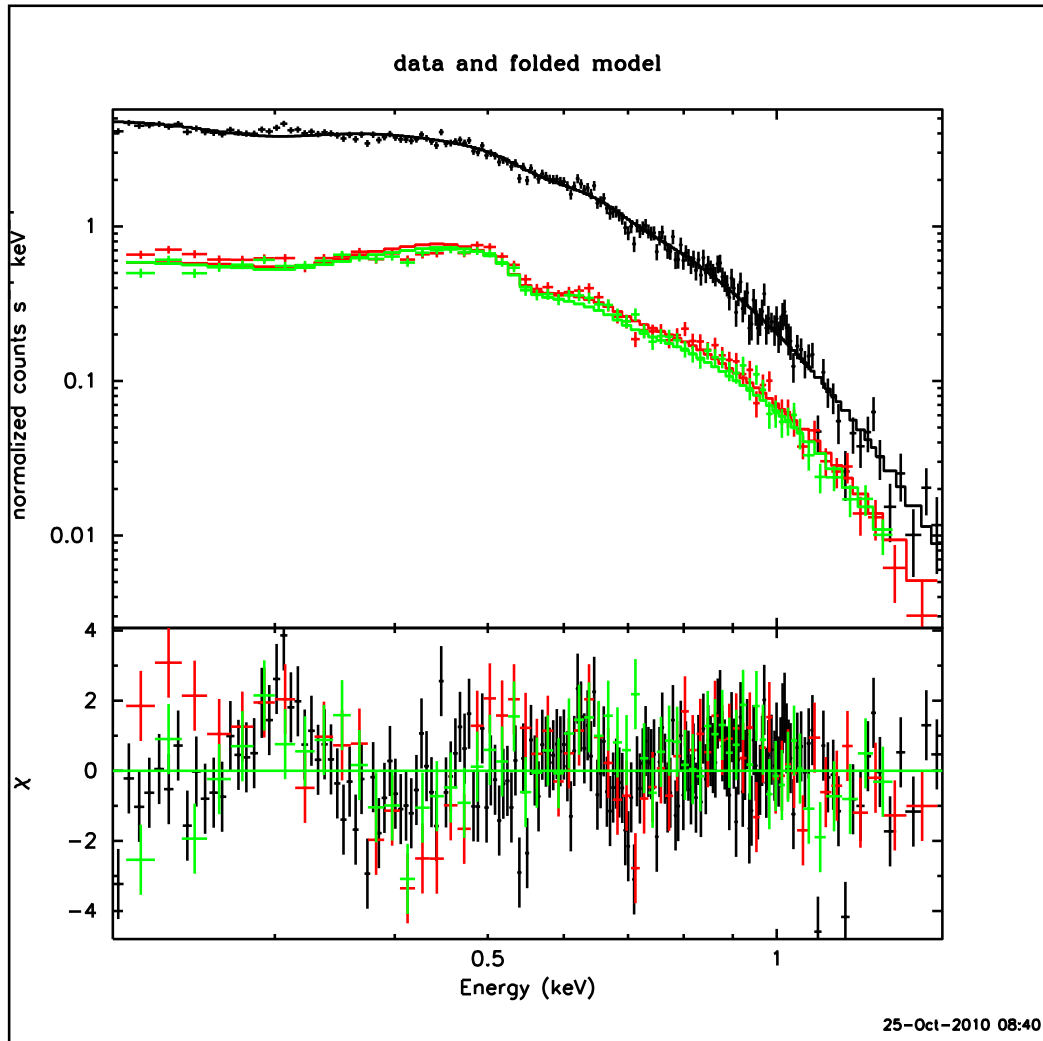


Figure 4.3: EPIC-pn and EPIC-MOS spectra of RBS1774 fitted with a model, including an absorption edge at ~ 0.7 keV.

Table 4.2: The model parameters of RBS1774 for combined fits to EPIC-pn and EPIC-MOS in the energy interval 0.2 – 1.5 keV. (The fitting results with a pure blackbody model absorbed by cold interstellar matter are from Schwope et al. (2009))

Model	n_H (10^{20} cm^{-2})	ϵ_m^{-1} (eV)	kT_{bb}^∞ (eV)	$E_{edge/line}$ (eV)	σ_{line} (eV)	$\tau_{edge/line}$	$\chi^2(\text{dof})$
plasma	$3.36_{-0.20}^{+0.20}$	7.0 ± 0.2					1.63(311)
plasma*edge	$3.30_{-0.12}^{+0.12}$	6.9 ± 0.1		679_{-13}^{+13}		$0.20_{-0.03}^{+0.03}$	1.50(309)
bbody	$1.85_{-0.17}^{+0.17}$		103.5 ± 0.8				1.81(311)
bbody*gabs	$1.84_{-0.17}^{+0.20}$		105.1 ± 0.9	731_{-13}^{+8}	27_{-4}^{+16}	$6.5_{-1.0}^{+1.2}$	1.50(308)

et al. (2009) if one uses the RGS X-ray spectra of RBS1774 in place of EPIC spectra, the resulting χ^2 is changed just marginally when a Gaussian absorption line is included at $\sim 0.7\text{keV}$. Thus, we conclude that the nature of the feature at 0.7keV is uncertain and might be related to calibration uncertainties of the CCDs and the RGS at those very soft X-ray energies. The same can be told about a feature at $\sim 0.3\text{keV}$ (the large residuals around 0.3keV are evident from inspection of Figs. 4.2 - 4.3). A feature of possible similar nature was detected in EPIC-pn spectra of the much brighter prototypical object RXJ1856 and classified as remaining calibration problem by Haberl (2007). Consequently, more data are necessary to finally prove or disprove the existence of those features.

4.3 Optical emission

The frequency of the original waves, excited during the cyclotron resonance can be estimated from Eq. (2.16) as follows

$$\nu \approx 2\pi \frac{\omega_B}{\delta\gamma_b} \sim 10^{14} \text{ Hz}. \quad (4.9)$$

As we can see the frequency of cyclotron modes comes in the same domain as the measured optical emission of RXJ1856 and RBS1774 (Burwitz et al., 2003; Zane et al., 2008; Schwope et al., 2009).

4.4 The effectiveness of the cyclotron mechanism

For effective generation of waves it is essential that the time during which the particles give energy to waves should be more than $1/\Gamma_c$. Generated waves propagate practically in straight lines, whereas the field line of the dipole magnetic field deviates from its initial direction, and the angle $\alpha = k_{\parallel}/k_{\varphi}$ grows. α is the angle between the wave line and the line of dipole magnetic field. On the other hand, the resonance condition (2.3) imposes limitations on $\alpha \approx \max\{\sqrt{\delta}, \frac{u_x}{c}\}$ (Kazbegi et al., 1991b); i.e. particles can resonate with the waves propagating in a limited range of angles. Obviously equation (2.3) will be fulfilled before (Lyutikov et al., 1999b):

$$\frac{c}{\Gamma_c} \lesssim \alpha\rho, \quad (4.10)$$

where $c\Gamma_c^{-1}$ is the growth length and $\alpha\rho$ the length of the wave-particle interaction. For the beam particles from equation (4.10), it follows that $\rho \gtrsim 3 \cdot 10^9 \text{cm}$. As the cyclotron instability arises at distances $r \sim 10^9 \text{cm}$ for the beam electrons, this result means that the time of wave interaction with the resonant particles is definitely enough for particles to acquire the pitch-angles, which automatically leads to the generation of synchrotron emission.

4.5 The recently discovered 7s pulsations of RXJ1856

Despite extensive searches, none of the previous analysis of the X-ray data of RXJ1856 revealed any significant periodicity (Pons et al., 2002; Ransom et al., 2002; Drake et al., 2002; Burwitz et al., 2003). Considering the case of a nearly aligned rotator, by Chkheidze & Machabeli (2007) it was predicted that the source should have pulsed with a period of ~ 1 s. However, the posterior XMM-Newton observation of RXJ1856 discovered that its X-ray emission pulsates with a period of 7.055 s (Tiengo & Mereghetti, 2007). The latter fact has been explained in the framework of drift wave driven model (Chkheidze & Lomiashvili, 2008). In particular, the real spin period of the pulsar might differ from the observable one, as a consequence of the

existence of very low frequency drift waves in the region of generation of the pulsar emission. These waves are not directly observable but only result in a periodical change of curvature of the magnetic field lines and, hence, a periodical change of the emission direction with a period of the drift waves assumed to be equal to the observable period (Lomiashvili et al., 2006).

4.5.1 Generation of drift waves

Under certain conditions the considered distribution function will generate various wave-modes. Particularly it has been shown (Kazbegi et al., 1991b, 1996) that very low frequency, nearly transverse drift waves can be excited. They propagate across the magnetic field, so that the angle between \mathbf{k} and \mathbf{B} is close to $\pi/2$. In other words, $k_{\perp}/k_{\varphi} \gg 1$, where $k_{\perp} = (k_r^2 + k_{\varphi}^2)^{1/2}$. Assuming $\gamma(\omega/\omega_B) \ll 1$, $(u_i/c)^2 \ll 1$, $k_{\varphi}/k_x \ll 1$ and $k_r \rightarrow 0$, we can write the general dispersion equation of the drift waves in the following form (Kazbegi et al., 1991a,b, 1996):

$$\begin{aligned} & \left(1 - \sum_i \frac{\omega_i^2}{\omega} \int \frac{u_i^2}{V_{\varphi} c \omega \omega - k_{\varphi} V_{\varphi} - k_x u_i} \frac{1}{\partial p} \frac{\partial f_i}{\partial p} dp - \frac{k_{\varphi}^2 c^2}{\omega^2} \right) \times \\ & \quad \times \left(1 + \sum_i \frac{\omega_i^2}{\omega} \int \frac{V_{\varphi}/c}{\omega - k_{\varphi} V_{\varphi} - k_x u_i} \frac{\partial f_i}{\partial p} dp \frac{k_{\varphi}^2 c^2}{\omega^2} \right) - \\ & \quad - \left(\frac{k_x k_{\varphi} c^2}{\omega^2} + \sum_i \frac{\omega_i^2}{\omega} \int \frac{V_{\varphi}/c}{\omega - k_{\varphi} V_{\varphi} - k_x u_i} \frac{\partial f_i}{\partial p} dp \right)^2 = 0, \end{aligned} \quad (4.11)$$

where i denotes the sort of particles (electrons or positrons) and $\omega_i^2 = 4\pi n_i e^2/m$, f_i is the distribution function and p is the momentum of the plasma particles.

Let us assume that

$$\omega = k_{\varphi} V_{\varphi} + k_x u_b + i\Gamma_{dr}, \quad (4.12)$$

where u_b is the drift velocity of the beam particles (see equation (2.2)). In the approximation $k_{\varphi} V_{\varphi} \ll k_x u_b$ and $k_x^2 \ll \omega_p^2/\gamma_p^3 c^2$, the imaginary part can

be written as:

$$\Gamma_{dr} = Im\omega \approx \left(\frac{n_b}{n_p}\right)^{1/2} \left(\frac{\gamma_p^3}{\gamma_b}\right)^{1/2} k_x u_b. \quad (4.13)$$

According to equation (4.12), the frequency of a drift wave can be written as

$$\omega_{dr} = Re\omega = k_\varphi V_\varphi + k_x u_b \approx k_x u_b. \quad (4.14)$$

Drift waves propagate across the magnetic field and encircle the region of the open field lines of the pulsar magnetosphere. They draw energy from the longitudinal motion of the beam particles, as in the case of the ordinary Cherenkov wave-particle interaction. However, they are excited only if $k_x u_b \neq 0$, i.e., in the presence of drift motion of the beam particles. Note that these low-frequency waves are nearly transverse, with the electric vector being directed almost along the local magnetic field. Let us note that although $k_\varphi V_\varphi \ll k_x u_b$ for the drift waves, there still exists a nonzero k_φ . It appears that growth rate (Eq. (4.13)) is rather small. However, the drift waves propagate nearly transversely to the magnetic field, encircling the magnetosphere, and stay in the resonance region for a substantial period of time. Although the particles give a small fraction of their energy to the waves and then leave the interaction region, they are continuously replaced by the new particles entering this region. The waves leave the resonance region considerably slower than the particles. Hence, there is no sufficient time for the inverse action of the waves on the particles. The accumulation of energy in the waves occurs without quasi-linear saturation. The amplitude of the waves grows until the nonlinear processes redistribute the energy over the spectrum. As was demonstrated by Kazbegi et al. (1991b), the strongest nonlinear process in this case is the induced scattering of waves on plasma particles. Therefore, the growth of the drift wave amplitude continues until the decrement of the nonlinear waves Γ_{NL} becomes equal to the linear decrement Γ_{dr} . As a result, one obtains quasi-regular configurations of drift waves. Generally, the nonlinear scattering pumps the wave energy into the long-wavelength domain of

the spectrum.

$$\lambda_{max} \approx r_{LC} = \frac{cP}{2\pi}. \quad (4.15)$$

Here r_{LC} is the radius of the light cylinder.

According to equations (4.14), (4.15) and (2.2), the period of the drift waves can be written as:

$$P_{dr} = \frac{e}{4\pi^2 mc} \frac{BP^2}{\gamma}, \quad (4.16)$$

It appears that the period of the drift waves can vary in a broad range. It is possible to determine the relationship between P_{dr} , the derivative and the rate of slowing down of the neutron star from equation (4.16)

$$\dot{P}_{dr} = \frac{eB}{2\pi^2 mc\gamma} P\dot{P}. \quad (4.17)$$

This relation is kept during the entire life of the pulsar, until it stops emitting.

4.5.2 Change of the field line curvature and the emission direction by the drift waves

Let us assume that a drift wave with the dispersion defined by equation (4.11) is excited at some place in the pulsar magnetosphere. It follows from the Maxwell equations that $B_r = E_\varphi(k_x c/\omega_0)$, hence $B_r \gg E_\varphi$ for such a wave. Therefore, excitation of a drift wave causes particular growth of the r -component of the local magnetic field.

The field line curvature $\rho \equiv 1/r$ is defined in a Cartesian frame of coordinates as

$$\rho = \left[1 + \left(\frac{dy}{dx} \right)^2 \right]^{-3/2} \frac{d^2y}{dx^2}, \quad (4.18)$$

where $dy/dx = B_y/B_x$. Using $(\nabla\mathbf{B}) = 0$ and rewriting equation (4.18) in the cylindrical coordinates we obtain

$$\rho = \frac{1}{r} \frac{B_\varphi}{B} - \frac{1}{r} \frac{1}{B} \frac{B_\varphi^2}{B^2} \frac{\partial B_r}{\partial \varphi}. \quad (4.19)$$

Here $B = (B_\varphi^2 + B_r^2)^{1/2} \approx B_\varphi[1 + (B_r^2/2B_\varphi^2)]$. Assuming that $k_\varphi r \gg 1$ we

obtain from equation (4.19)

$$\rho = \frac{1}{r} \left(1 - k_\varphi r \frac{B_r}{B_\varphi} \right). \quad (4.20)$$

From equation (4.20) it is clear that even a small change of B_r causes significant change of ρ . Indeed, based on the dimensional estimations, we can write $k_\varphi r \gg 2\pi$, and variation of the field line curvature can be estimated as

$$\frac{\Delta\rho}{\rho} \approx k_\varphi r \frac{\Delta B_r}{B_\varphi}, \quad (4.21)$$

It follows that even a drift wave with a modest amplitude $B_r \sim \Delta B_r \sim 0.01 B_\varphi$ alters the field line curvature substantially $\Delta\rho/\rho \sim 0.1$.

Since the pulsar emission propagates along the local magnetic field lines, curvature variation causes change of the emission direction, with the period of the drift waves.

4.5.3 The model

There is a direct correspondence between the observable intensity and α (the angle between the line of sight of an observer and the magnetic axis, see Fig. 4.4). The maximum of intensity corresponds to the minimum of α . The period of the pulsar is then the time interval between neighboring maxima of the observable intensity i.e. minima of α . According to this fact, we can say that the observable period depends on the time behavior of α and as the observable period appears below it might differ from the 'real' spin period of the pulsar. From pulsar geometry it follows that α can be expressed as (Lomiashvili et al., 2006):

$$\cos \alpha = \vec{k} \vec{\mu}, \quad (4.22)$$

where \vec{k} and $\vec{\mu}$ are unit guide vectors of observers and magnetic axes, respectively. In the spherical coordinate system (r, φ, θ) combined with the plane

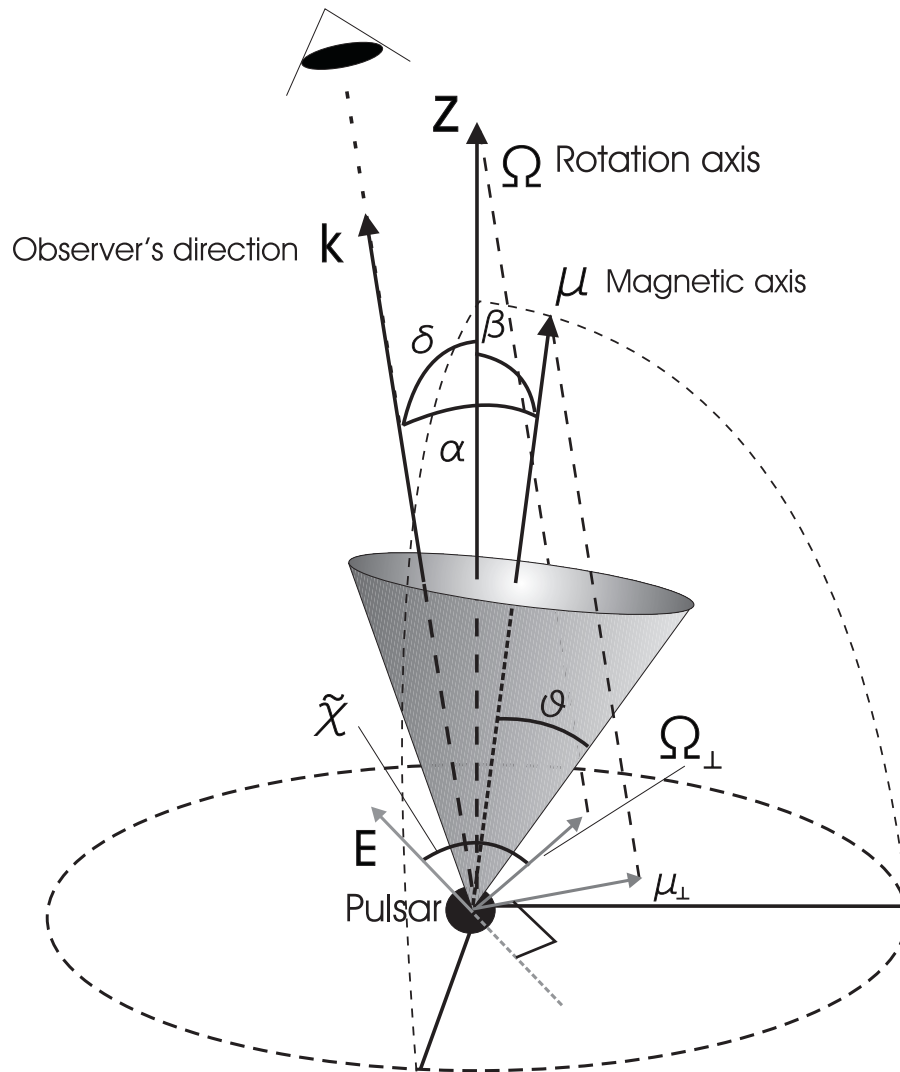


Figure 4.4: $\vec{\Omega}$ is the rotation axis, $\vec{\mu}$ - the magnetic-moment axis, \vec{k} - the observer's axis and \vec{E} is the electric field vector of the radiation. $\vec{\mu}_\perp$ and $\vec{\Omega}_\perp$ are the projections of the corresponding vectors on the plane of sky, $\tilde{\chi}$ is the position angle.

of the pulsar rotation, these vectors can be expressed as:

$$\begin{aligned}\vec{k} &= (1, 0, \delta), \\ \vec{\mu} &= (1, \Omega t, \beta),\end{aligned}\tag{4.23}$$

where $\Omega = 2\pi/P$ is the angular velocity of the pulsar, $\omega_{dr} = 2\pi/P_{dr}$ is the cyclic frequency of the drift wave, δ is the angle between the rotation and the observer's axis, β is the angle between the rotation and magnetic-moment axis (see Fig. 4.4).

From equations (4.22) and (4.23), it follows that:

$$\alpha = \arccos(\sin \delta \sin \beta \cos \Omega t + \cos \delta \cos \beta).\tag{4.24}$$

In the absence of the drift wave $\beta = \beta_0 = \text{const}$ and consequently the period of α equals $2\pi/\Omega$.

According to equation (4.21), in the presence of the drift wave, the fractional variation $\Delta\rho/\rho$ is proportional to the magnetic field of the wave B_r , which is periodically changing. So $\beta = \beta(t)$ is harmonically oscillating about β_0 with an amplitude $\Delta\beta = \Delta\rho/\rho$ and rate $\omega_{dr} = 2\pi/P_{dr}$. Thus, we can write that

$$\beta = \beta_0 + \Delta\beta \sin(\omega_{dr}t + \varphi).\tag{4.25}$$

According to equations (4.24) and (4.25) we obtain

$$\begin{aligned}\alpha &= \arccos[\sin \delta \sin(\beta_0 + \Delta\beta \sin(\omega_{dr}t + \varphi)) \cos \Omega t + \\ &\quad + \cos \delta \cos(\beta_0 + \Delta\beta \sin(\omega_{dr}t + \varphi))],\end{aligned}\tag{4.26}$$

If the angle between the rotation and emission axes is very small i.e. $\delta \ll 1$, then the period of α equals $P_{dr} = 2\pi/\omega_{dr}$. In this case the observable period P_{obs} does not represent the real spin period of the pulsar, but equals the period of the drift wave, which we assume to be 7.055 s. When the real spin period of this object has been estimated by Chkheidze & Machabeli (2007) to be $P \approx 1s$.

Hence, for some values of parameters β , $\Delta\beta$, δ , φ and ϑ (here ϑ is the

opening angle of the X-ray emission cone) it is possible to explain the observed 7 s pulsations of RXJ1856. The observations detect continuous radiation meaning that the following condition: $\alpha(t) \leq \vartheta$, has to be fulfilled at any moment of time. The posterior results depend on the angular size of the X-ray emission cone. For the primary beam electrons (which generate the observed X-ray emission), the distribution function by their pitch angles has the form expressed by equation $f_{\perp}(\psi) \propto e^{-A\psi^4}$ (see Eq. (2.42), where $\psi = p_{\perp}/p_{\parallel}$) and $A \simeq 10^{10}$ (the mean value of the pitch angle estimates as $\psi_0 \simeq 10^{-3}$). The greatest possible value of the pitch angle, acquired by the beam of electrons at the quasi-linear stage of the cyclotron instability, is of the order of ψ_0 . The electron emits in the direction of motion through a small cone with the opening angle $1/\gamma$, which for the primary beam electrons is $\simeq 10^{-7}$ and the magnetic field lines are nearly parallel and straight in the emitting region. Thus, we conclude that the angular size of the emission cone is equal to the maximal possible value of the pitch angle of the emitting electrons. It means that the opening angle of the X-ray emission cone should be $\vartheta \simeq 10^{-3}$.

The emission intensity undergoes periodic variations due to the star's rotation. The emission intensity in the given direction is defined as follows (Ginzburg, 1981):

$$I(\nu) = \frac{3e^3}{2\pi} \int B \left(\frac{\nu}{\nu_c} \right)^2 (1 + \chi^2 \gamma^2) \gamma f(\gamma, \psi) \sin \alpha \times \\ \times \left[K_{2/3}^2(g_{\nu}) + \chi^2 \gamma^2 K_{1/3}^2(g_{\nu}) \right] d\chi d\gamma. \quad (4.27)$$

Its time dependence can be approximately expressed in the following form:

$$I(t) \propto \sin \alpha e^{-A(\alpha+\chi)^4}. \quad (4.28)$$

Here the expression $\psi = \alpha + \chi$ has been taken into account (χ is the angle between the wave vector and the velocity vector of the emitting electron, see Fig. 4.5). The angle $\alpha \sim 10^{-3}$, while the maximal value of the angle χ is $\sim 10^{-7}$, consequently we can approximately write

$$I(t) \propto \sin \alpha e^{-A\alpha^4}. \quad (4.29)$$

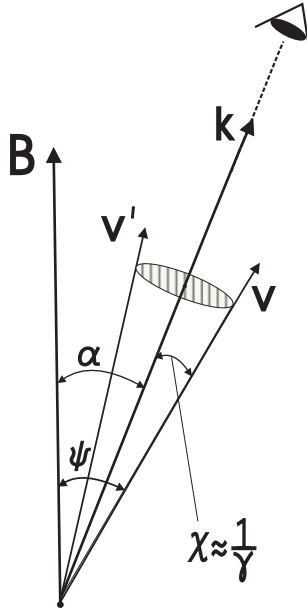


Figure 4.5: \mathbf{k} is the emission direction, \mathbf{B} - the magnetic field line, \mathbf{v} and \mathbf{v}' - are the electrons' velocities.

The fitting is done with the observational data, using this expression for the emission intensity. The simulated light curves for RXJ1856 are presented in Fig. 4.6, with two different values for the angle δ . As we can see the value of the pulsed fraction of only $\sim 1.2\%$ is well expressed and the data is well fitted. The change of δ causes the appearance of additional peaks correspondent to the pulsations with a real spin period approximately equaled to 1 s. Therefore, we expect that the detection of the 'real' spin period of RXJ1856 can be achieved with observations of higher resolution. In Fig. 4.7 the change of α in time is presented, as we can see the condition $\alpha(t) \leq 10^{-3}$ is fulfilled at any moment of time. The values for the angular parameters obtained from fitting are presented in Table 4.3.

Assuming the star is spinning down by magnetic dipole radiation, one can use the spin-down rate to infer a magnetic field strength. The dipolar magnetic field strength at the neutron star surface can be written as:

$$B_0 \simeq 3.2 \times 10^{19} \sqrt{\dot{P}P} \quad (4.30)$$

According to van Kerkwijk & Kaplan (2008) the observed value of the period and period derivative are $P_{obs} \approx 7\text{s}$, $\dot{P}_{obs} \simeq 3 \cdot 10^{14} \text{ss}^{-1}$. These measured quantities represent the period and period derivative of the drift waves, when

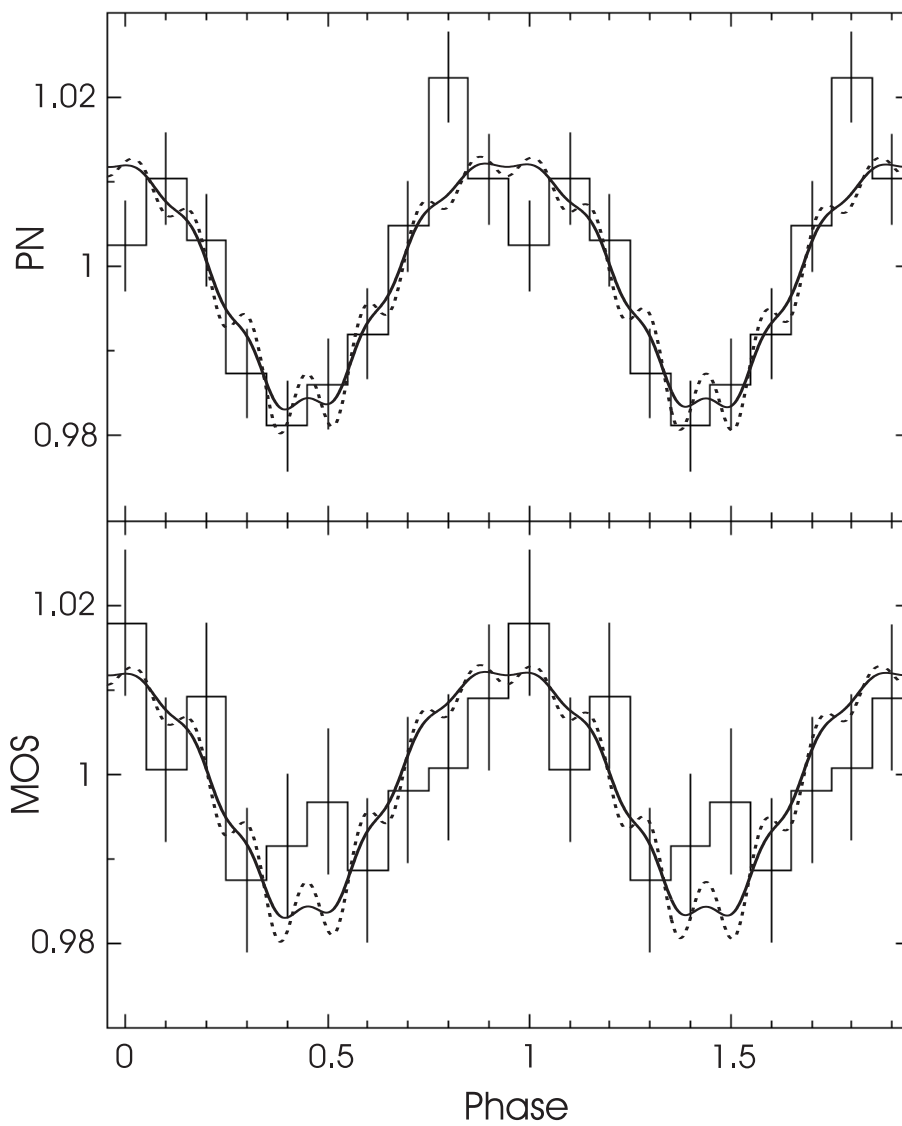


Figure 4.6: The simulated light curves of RX J1856.5-3754 fitted with PN and MOS observations. The solid and the dotted lines correspond to $\delta \sim 10^{-6}$ and $\delta \sim 10^{-5}$, respectively.

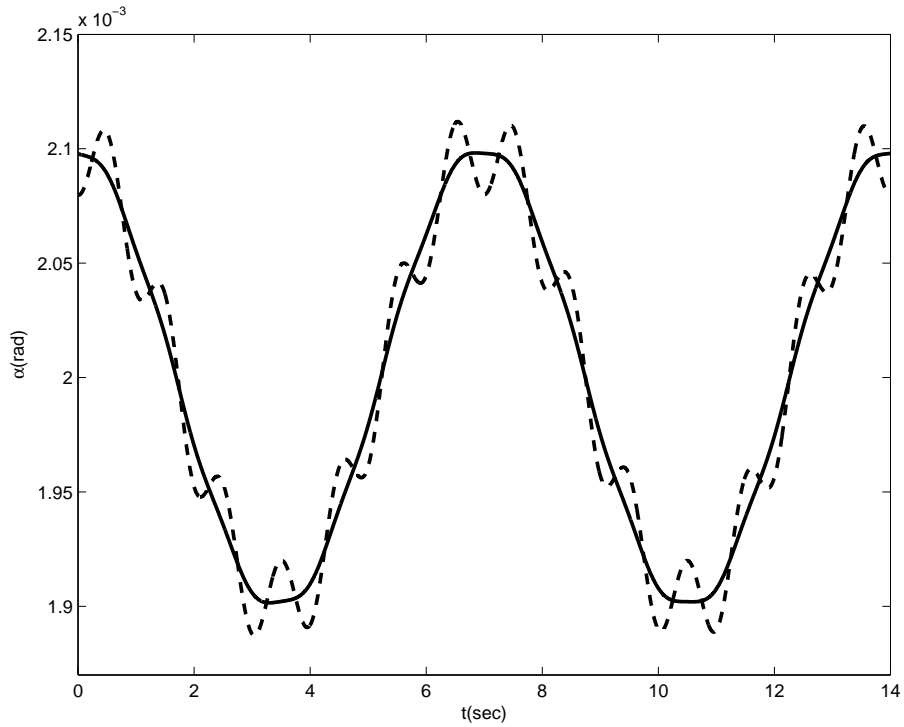


Figure 4.7: Oscillating behaviour of α with time. The solid and the dotted lines correspond to $\delta \sim 10^{-6}$ and $\delta \sim 10^{-5}$, respectively.

Table 4.3: The values of angular parameters for RX J1856.5-3754.

$P_{obs}(s)$	$P(s)$	$\Delta\beta$	β_0	δ	ϑ
7.055	1.5	10^{-4}	$2 \cdot 10^{-3}$	$2 \cdot 10^{-5}$	10^{-3}

the real spin period and its derivative can be obtained from equations (4.16) and (4.17). As we have already estimated the real spin period is $\approx 1s$, thus, the value for the real spin period derivative will be $\dot{P} \simeq 2 \cdot 10^{-15}ss^{-1}$. Using the latter values one can get the magnetic field strength at the pulsar surface $B_0 \simeq 10^{12}G$.

4.6 The polarization properties of RXJ1856

We are not about to reject the existing thermal radiation models for RXJ1856 and suppose that the most reliable argument for revealing the real emission nature of this source will be its study with polarization instruments. Therefore in this section the polarization properties of RXJ1856 are investigated, in the framework of the plasma emission model (see Chkheidze (2009)).

4.6.1 Emission polarization

Let us consider the emission polarization of RXJ1856. For this reason, we have to find the Stokes parameters, which, in our case, are defined as follows (Ginzburg, 1981):

$$I(\nu) = \frac{3e^3}{2\pi} \int B \left(\frac{\nu}{\nu_c} \right)^2 (1 + \chi^2 \gamma^2) \gamma f(\gamma, \psi) \sin \alpha \times \\ \times \left[K_{2/3}^2(g_\nu) + \chi^2 \gamma^2 K_{1/3}^2(g_\nu) \right] d\chi d\gamma, \quad (4.31)$$

$$Q(\nu) = \frac{3e^3}{2\pi} \int B \left(\frac{\nu}{\nu_c} \right)^2 (1 + \chi^2 \gamma^2) \gamma^2 f(\gamma, \psi) \sin \alpha \cos 2\tilde{\chi} \times \\ \times \left[K_{2/3}^2(g_\nu) - \chi^2 \gamma^2 K_{1/3}^2(g_\nu) \right] d\chi d\gamma, \quad (4.32)$$

$$U(\nu) = \frac{3e^3}{2\pi} \int B \left(\frac{\nu}{\nu_c} \right)^2 (1 + \chi^2 \gamma^2) \gamma^2 f(\gamma, \psi) \sin \alpha \sin 2\tilde{\chi} \times \\ \times \left[K_{2/3}^2(g_\nu) - \chi^2 \gamma^2 K_{1/3}^2(g_\nu) \right] d\chi d\gamma, \quad (4.33)$$

$$V(\nu) = \frac{3e^3}{\pi} \int B \left(\frac{\nu}{\nu_c} \right)^2 (1 + \chi^2 \gamma^2)^{3/2} \gamma^2 \chi f(\gamma, \psi) \sin \alpha \times \\ \times K_{1/3}(g_\nu) K_{2/3}(g_\nu) d\chi d\gamma, \quad (4.34)$$

here the angle $\tilde{\chi}$ defines the direction of maximum intensity of the polarized component on the plane of sky.

Synchrotron emission of a single electron is strongly beamed along the direction of motion into an angle of order $1/\gamma$. Hence, in the given direction, the observer will detect radiation of the electrons with velocities filling up the cone with $1/\gamma$ in angular size and with the major axis coincided with the line of sight of an observer (see Fig. 4.5). Therefore, at the given moment of time, the observer receives emission of the electrons having the pitch-angles from the interval $\psi = \alpha + \chi \subset [\alpha - 1/\gamma, \alpha + 1/\gamma]$ (it should be mentioned

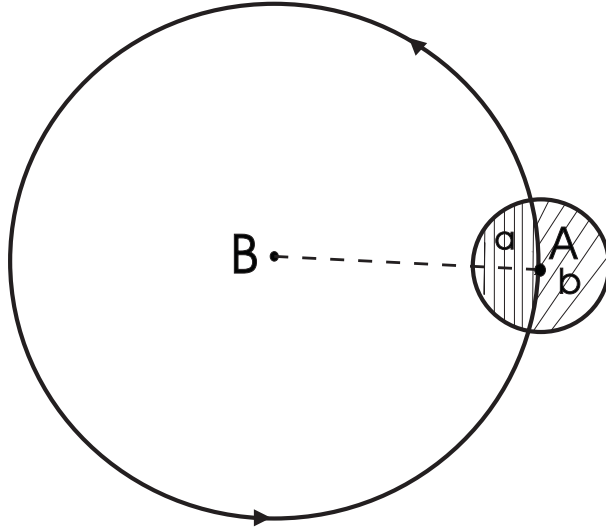


Figure 4.8: Point **B** corresponds to the magnetic field line and point **A** - to the observer's line of sight.

that the angle χ is considered to be positive if $\psi > \alpha$ and to be negative, otherwise). The Stokes parameter V is an odd function of variable χ , therefore, its integration over symmetric interval yields zero. Let us consider the top view of Fig. 4.5 (see Fig. 4.8). The larger circle represents a cross section of the cone. The lateral surface of this cone is described by the electron velocity vector moving on a spiral along the magnetic field line. The circle with smaller radius corresponds to the cone combined by the velocity vectors giving the significant radiation in the observer's direction. Its angular size estimates as $1/\gamma$. The area of the smaller circle is striped in two different ways: area **a** corresponds to the electrons which have positive values of angle χ , while area **b** corresponds to those having negative values of angle χ . As these areas are not equal to each other, one would expect the nonzero value of V . But bearing in mind that the bigger circle is large enough in comparison with the smaller one (the solid angles of corresponding cones are of the order of 10^{-3} and 10^{-7} for the beam electrons), one can easily assume that $\mathbf{a} \approx \mathbf{b}$. But only symmetry of integration bounds is not enough condition to have a zero circular polarization. Also the distribution function by pitch angles, containing the variable χ , should change very slowly within the small interval $\sim 1/\gamma$. The estimations show that the latter condition is well fulfilled. Thus, we conclude that the emission of this source is not circularly polarized.

Now we can calculate the degree for the linear polarization, which writes as (Ginzburg, 1981):

$$\Pi_l = \frac{\sqrt{Q^2 + U^2}}{I}. \quad (4.35)$$

The degree of linear polarization, corresponding to the energy interval (0.15–0.85)keV of the observed X-ray spectrum can be calculated using equations (2.42), (4.1), (4.31), (4.32) and (4.33), we get $\Pi_l \approx (84 - 79)\%$.

4.6.2 Position angle

It is very important to know the behaviour of the PA (Position angle) of linear polarization of the X-ray emission through the pulse. If we use spherical coordinate system (r, φ, θ) (see Fig. 4.4), then we write:

$$\begin{aligned} \vec{k} &= (1, 0, \delta), \\ \vec{\mu} &= (1, \Omega t, \beta), \\ \vec{\Omega} &= (1, 0, 0). \end{aligned} \quad (4.36)$$

Here \vec{k} , $\vec{\mu}$ and $\vec{\Omega}$ are unit guide vectors of observers, magnetic and rotation axes, respectively. As we know, the PA is an angle between the electric field of radiation and the projected spin axis on the plane of sky. From Fig. 4.9, it is easy to find the expression for PA, which has the following form:

$$\tilde{\chi} = \frac{\pi}{2} - \arccos \left(\frac{\cos \beta - \cos \alpha \cos \delta}{\sin \alpha \sin \delta} \right), \quad (4.37)$$

where α is defined from expression (4.26). If we take for the value of the real spin period $P = 1.5\text{s}$, we can see that the PA rotates by 360° for a few times within the observable period, as the star makes more than one rotation in 7.055s (see Fig. 4.9).

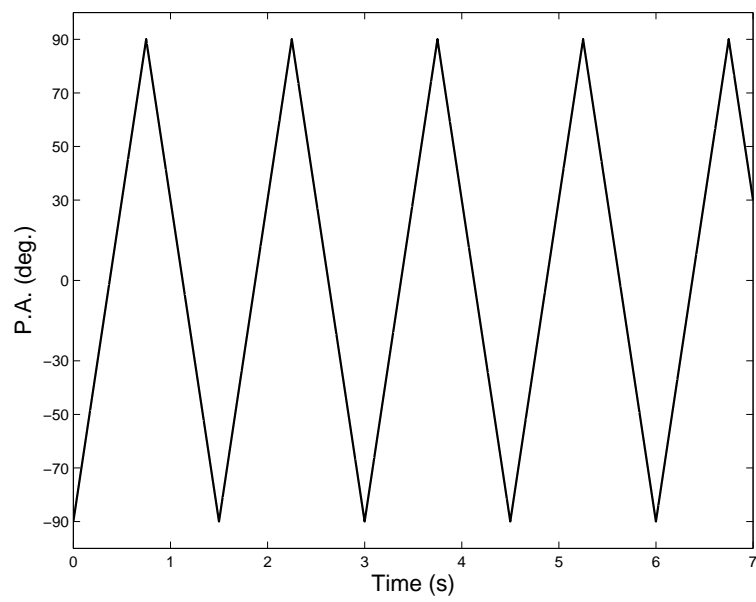


Figure 4.9: The behaviour of the position angle of the linearly polarized X-ray emission within one observable pulse.

Chapter 5

The HE energy pulsed emission of PSR B0531+21

The recent observations of the MAGIC Cherenkov telescope (Aliu et al., 2008), reveal several characteristic features of the HE emission of the Crab pulsar. In particular, pulsed γ -rays above 25GeV is detected showing a relatively HE cutoff, which indicates that emission happens far out in the magnetosphere (Aliu et al., 2008). The pulsar emission model that underlies our work, provides the generation of the observed emission in the outer part of the pulsar magnetosphere (the region near the light cylinder). As we have already outlined in the electron-positron plasma of a pulsar magnetosphere the low frequency cyclotron modes (which come in the radio domain (Chkheidze et al., 2010)), on the quasi-linear evolution stage create conditions for generation of the HE synchrotron emission. A special interest deserves the coincidence of signals from different frequency bands ranging from radio to X-rays (Manchester & Taylor, 1980). Investigations of last decade have shown that the aforementioned coincidence takes places in the HE domain (0.01MeV-25GeV) as well (Aliu et al., 2008). In the framework of the present work, generation of low and high frequency waves is a simultaneous process and it takes place in one location of the magnetosphere, which explains the observed pulse phase coincidence of the low and HE signals. Consequently, we suppose that generation of phase-aligned signals from different frequency

bands is a simultaneous process and it takes place in one location of the pulsar magnetosphere. This in turn, restricts possibility of choice of radiation mechanisms and as recently has been shown by Machabeli & Osmanov (2009, 2010), the ICS and the curvature radiation should be excluded, which are not localized.

5.1 Synchrotron HE spectrum of the Crab pulsar

It is well known that close to the pulsar surface due to very strong magnetic fields, magnetospheric particles emit efficiently and the corresponding cooling timescale is short compared to the typical kinematic timescales of particles. Therefore, transversal energy loss becomes extremely efficient, consequently electrons and protons lose their perpendicular momenta and very rapidly transit to their ground Landau states and the distribution function becomes one dimensional. This means that one needs a certain mechanism, leading to the creation of the pitch angles restoring the synchrotron radiation. The main mechanism of wave generation in plasmas of the pulsar magnetosphere is the cyclotron instability (Kazbegi et al., 1992). During the quasi-linear stage of the instability, a diffusion of particles arises along and across the magnetic field lines. Therefore, the resonant electrons acquire transverse momenta and, as a result start to radiate in the synchrotron regime. We assume that the observed HE spectrum of the Crab pulsar is the result of the synchrotron emission of the primary beam electrons. According to the expression (3.26) the beam electrons should have $\gamma_b \simeq 6 \cdot 10^8$ to radiate the photons with $\sim 10\text{GeV}$ energy. This in turn implies that the gap models providing the Lorentz factors $\sim 10^7$, are not enough to explain the detected pulsed emission. On the other hand, Aliu et al. (2008) confirmed that their observations indicate that emission happens far out in the magnetosphere. One of the real scenarios could be the centrifugal acceleration of electrons, which takes place in co-rotating magnetospheres (Machabeli & Rogava, 1994; Rogava et al., 2003; Osmanov et al., 2007). Another alternative mechanism of acceleration could be a collapse (Artsimovich & Sagdeev, 1979; Zakharov,

1972) of the centrifugally excited unstable Langmuir waves (Machabeli et al., 2005) in the pulsar magnetosphere.

According to Aliu et al. (2008) the observed high energy pulsed emission of the crab pulsar is best described by a power-law spectrum $F(\epsilon) \propto \epsilon^{-2.022}$ in the energy domain (0.01 – 5)GeV. At $\epsilon = 25\text{GeV}$ a measured flux is several times lower, which requires a spectral cutoff somewhere between 5 and 25GeV.

We assume that the energy of the beam electrons vary between $\gamma_{min} \sim 10^6$ and $\gamma_{max} \sim 10^8$, in which case, we have $(\epsilon/\epsilon_m)_{max} \ll 1$ and $(\epsilon/\epsilon_m)_{min} \gg 1$. Under such conditions the integral (3.41) can be approximately expressed by the following function

$$F_\epsilon \propto \epsilon^{-\frac{2-n}{4-n}} \exp \left[- \left(\frac{\epsilon}{23} \right)^{1.6} \right]. \quad (5.1)$$

When $n = 6$ (which means that the initial energy distribution of the beam electrons $f_{||0} \propto p_{||}^{-6}$) the spectral index, β , of the synchrotron emission equals 2, and the flux $F_\epsilon \propto \epsilon^{-2} \exp[-(\epsilon/23)^{1.6}]$. As we can see our emission scenario predicts the exponential cutoff, with the cutoff energy 23GeV.

The frequency of the original waves, excited during the cyclotron resonance can be estimated from expression (2.16). Estimations show that for the beam electrons with the Lorentz-factor from the interval $\gamma_b \sim 10^{6-8}$, the radio waves are excited. Consequently, we explain the coincidence of radio and γ -ray signals.

As we see, the synchrotron emission can explain the observed HE radiation, and as we have already seen, for this purpose the particles must have very high Lorentz factors. On the other hand, these particles will inevitably encounter soft photons, which in turn can also create the high energy radiation via the ICS. But in this case the emission will not be localized contrary to the observational evidence, indicating that for some reason the ICS is not involved in the process of the detected emission. This particular problem was considered in (Machabeli & Osmanov, 2010), where analyzing the ICS, it has been demonstrated that for reasonable physical parameters even very

energetic electrons are unable to produce the photon energies of the order of 25GeV. The next section is dedicated to this particular problem.

5.2 Compton scattering

It is well known that when a photon with energy ϵ encounters a relativistic electron, under certain conditions photons might gain energy. The corresponding frequency after scattering is given by (Rybicki & Lightman, 1979)

$$\omega' = \omega \frac{1 - \beta \cos \theta}{1 - \beta \cos \theta' + \frac{\hbar\omega}{\gamma mc^2}(1 - \cos \theta'')}, \quad (5.2)$$

where ω is the frequency before scattering, $\beta \equiv v/c$, $\theta = (\mathbf{P}\hat{\mathbf{K}})$, $\theta' = (\mathbf{P}\hat{\mathbf{K}}')$, $\theta'' = (\mathbf{K}\hat{\mathbf{K}}')$. By \mathbf{K} and \mathbf{K}' we denote the three momentum of the photon before and after scattering, respectively. The momentum of relativistic electrons before scattering is denoted by \mathbf{P} .

Since, according to the observational evidence, we observe the well localized pulses of HE emission, therefore the angle, θ must be very small. On the other hand, analyzing the excitation of oblique waves in a relativistic electron-positron plasma one can argue that the pitch angle has to be extremely low (Volokitin, Krasnoselskikh & Machabeli, 1985). We will study two principally different cases: (a) $\cos \theta' \ll 1$ and (b) $\cos \theta' \sim 1$. In the first case we have

$$\omega' \approx \frac{\omega}{2\gamma^2} \times \frac{1}{1 + \frac{\hbar\omega}{\gamma mc^2}(1 - \cos \theta'')}, \quad (5.3)$$

where the following approximate relation, $1 - \beta \approx 1/2\gamma^2$ has been taken into account, for $\beta \sim 1$. From this expression we see that for all physical quantities the frequency after the scattering is less than that before the scattering and therefore, there is no possibility of increasing ω to the high energy band.

By considering the second limit, Eq. (5.2) reduces to

$$\omega' \approx \omega \frac{1}{1 + \frac{\hbar\omega}{\gamma mc^2}(1 - \cos \theta'')}, \quad (5.4)$$

which, as in the previous case, leads to the similar result, $\omega' < \omega$.

This investigation shows that the ICS cannot provide the HE radiation from the Crab pulsar detected by MAGIC (Aliu et al., 2008).

5.3 Curvature radiation

Since particles are moving along the curved magnetic field lines continuously, they will emit the curvature radiation. On the other hand, in Eq. (3.27) we have neglected a term corresponding to the curvature emission. This means that the following ratio

$$\eta \equiv \frac{\epsilon_{curv}}{\epsilon_{syn}}, \quad (5.5)$$

where (Ruderman & Sutherland, 1975)

$$\epsilon_{curv} = \frac{3\hbar}{2} \gamma_b^3 \frac{c}{\rho}, \quad (5.6)$$

must be less than one. By applying Eqs. (3.26), (5.5) and (5.6), one can show that for typical magnetospheric parameters of the Crab pulsar close to the light cylinder, the aforementioned ratio is negligible only if the curvature radius exceeds the light cylinder radius, R_{lc} , approximately by three orders of magnitude.

Generally speaking, since no contribution in emission comes from the closed magnetic field lines, we consider the open ones. On the other hand, in the dipolar field the region of almost straight field lines is just a tiny fraction of the emission area, leading to a negligible value of the high energy luminosity.

If the beam component particles move along curved field lines, they experience the so-called curvature drift with the velocity:

$$u_b = \frac{\gamma_{b0} v_{\parallel}^2}{\omega_{B_b} \rho}, \quad (5.7)$$

where $\omega_{B_b} = eB_0/mc$, B_0 is the background magnetic field induction. This velocity will eventually create the drift current, $J_{dr} = en_b u_b$ which in turn,

via the Maxwell equation

$$(\nabla \times B)_x = \frac{4\pi}{c} J_{dr}, \quad (5.8)$$

can create the toroidal magnetic field (by x we denote a direction of the drift current. See Fig. 1 in Appendix). This current is evidently less than the Goldreich-Julian (GJ) current $J_{GJ} = en_b c$, since $u_b \ll c$. But on the other hand, the GJ current creates the corresponding magnetic field, $B_r \approx 4\pi J_{GJ} R_n / c$, where $R_n \approx B(R) / B'(R) = R/3$ ($B' \equiv dB/dR$) is the length scale of the spatial inhomogeneity of the magnetic field. If we assume a dipolar configuration, then, by taking the value of the GJ density, $n_b \approx \Omega B / (2\pi e c)$ into account, one can show that the toroidal magnetic field equals $B(2R/3R_{lc})$. Inside the light cylinder ($R < R_{lc}$), this value is less than the background magnetic field- B and therefore such a toroidal magnetic field will be unable to rectify the twisted magnetic field lines. This implies that the curvature drift current, which is less than that of the GJ, cannot contribute to the process of rectifying the field lines. However, in spite of that the drift current is not the source of the toroidal component, B_r , it is a trigger mechanism for generating the perturbed current, $J_1 = e(n_b^0 v_{b_x}^1 + n_b^1 u_b)$ responsible for the creation of B_r (see Eq. (10)), where by upper script '1' we denote the perturbed quantities. The source of the instability of current and the resulting magnetic field is the pulsars rotational energy and the process is achieved via the parametrically excited curvature drift waves. The corresponding increment of the curvature drift instability (CDI) can be presented by (see Appendix, for more details see (Osmanov et al., 2009a,b)):

$$\Gamma \approx \left(-\frac{3 \omega_b^2 k_x u_b}{2 \gamma_{b_0} k_\theta c} \right)^{1/2} \left| J_0 \left(\frac{k_x u_b}{4\Omega} \right) J_0 \left(\frac{k_\theta c}{\Omega} \right) \right|, \quad (5.9)$$

where ω_b is the beam component plasma frequency and γ_{b_0} - the Lorentz factor in an unperturbed state. k_x and k_θ are the wave vectors components and Ω is the angular velocity of rotation.

By considering the typical magnetospheric parameters for the Crab pulsar close to the light cylinder, $P = 0.033$ s, $\gamma_{b_0} = 10^8$ and examining the per-

turbation lengthscale $\lambda \approx 10^8 \text{cm}$ (Osmanov et al., 2009a), one can see that the increment is of the order of 1s^{-1} . Comparing this value with the Crab pulsars slowdown rate, $4.2 \cdot 10^{-13} \text{s}^{-1}$, we see that the instability growth rate exceeds by many orders the magnitude of slowdown rate, indicating that the mentioned instability is extremely efficient.

It is worth noting that we have three types of the open field lines: (a) curved field lines which pass ahead of the rotation; (b) a tiny fraction of almost straight field lines and (c) curved field lines, lagging behind the rotation.

If the initial perturbation of the toroidal magnetic field satisfies the condition $B_r > 0$, then such a perturbation will rectify all field lines which initially pass ahead of the rotation (suppose the clockwise rotation of the system) and will twist even more the magnetic field lines, which initially lag behind the rotation. In the case, $B_r < 0$, the situation is opposite: the field lines initially lagging behind the rotation will be rectified. At this stage the curvature becomes infinity and as we see from Eq. (5.7), the drift velocity tends to zero, saturating (killing) the instability.

The investigation shows that, the CDI provides necessary conditions for an efficient mechanism of rectifying the field lines, leading to the negligible role of the curvature radiation.

Chapter 6

Discussion and Conclusions

In the present work the pulsar emission model is presented, which is based on well developed theory of pulsars. It is supposed that the relatively high energy pulsar emission is generated by the synchrotron mechanism. The distribution function of relativistic particles is one dimensional at the pulsar surface, but plasma with an anisotropic distribution function is unstable which can lead to wave excitation. The main mechanism of wave generation in plasmas of the pulsar magnetosphere is the cyclotron instability. During the quasi-linear stage of the instability, a diffusion of particles arises along and across the magnetic field lines. Therefore, plasma particles acquire transverse momenta and, as a result, the synchrotron mechanism is switched on.

In the framework of the model we explain the observational properties of three individual pulsars. In particular, the HE spectrum of the Crab pulsar is assumed to be the result of the synchrotron emission of the beam electrons, which start to radiate near the light cylinder, due to the cyclotron instability. If the resonant particles are the primary beam electrons with $\gamma_b \simeq 6 \cdot 10^8$ their synchrotron emission comes in the HE domain ($\sim 10\text{GeV}$). We provide the theoretical confirmation of the measured power-law spectrum ($F_\epsilon \propto \epsilon^{-\beta}$ with $\beta = 2$) in the energy domain $\epsilon = 0.01\text{GeV}$ to 25GeV . Differently from the standard theory of the synchrotron emission (Ginzburg, 1981), we take into account the mechanism of creation of the pitch angles, and obtain a certain

distribution function of the emitting particles from their perpendicular momenta, which restricts the possible values of the pitch angles. The emission comes from a region of the pulsar magnetosphere where the magnetic field lines are practically straight and parallel to each other. But in the standard theory of the synchrotron emission (Ginzburg, 1981), it is supposed that the observed radiation is collected from a large spacial region in various parts of which, the magnetic field is oriented randomly. Thus, it is supposed that along the line of sight the magnetic field directions are chaotic and when finding emission flux, Eq. (3.18) is averaged over all directions of the magnetic field (which means integration over ψ varying from 0 to π). The measured decrease of the flux at $\epsilon = 25\text{GeV}$ is also explained. Our theoretical spectrum $F_\epsilon \propto \epsilon^{-2} \exp[-(\epsilon/23)^{1.6}]$ yields the exponential cutoff, with the cutoff energy 23GeV .

One of the interesting observational feature of the Crab pulsar is that its multiwavelength emission pulses from low-frequency radio waves up to hard γ -rays ($\epsilon > 25\text{GeV}$) are coincident in phase (Manchester & Taylor, 1980; Aliu et al., 2008). Which implies that generation of these waves occurs in the same place of the pulsar magnetosphere. The present model ensures the simultaneous generation of the low and high frequency waves in the same area of the magnetosphere. The frequency of the original waves, excited during the cyclotron resonance is $\omega \approx \omega_B/\delta\gamma_b$. Estimations show that for the beam electrons with the Lorentz-factor from the interval $\gamma_b \sim 10^{6-8}$, the radio waves are excited. Consequently, we explain the coincidence of radio and γ -ray signals.

According to the generally accepted point of view, HE emission is produced either by the Inverse Compton up-scattering or by the curvature radiation. Although it is clear that the aforementioned processes cannot provide the observationally evident coincidence of signals, since they do not have any restriction on the spacial location of emission area. This particular problem has been studied by Machabeli & Osmanov (2010). Considering the curvature radiation, we have shown that the CDI (see Osmanov et al. (2008); Osmanov et al. (2009b)) makes the magnetic field lines rectify very efficiently, leading to

a negligible role of the curvature emission process in the observed HE domain. By analyzing the ICS, we have found that for Crab pulsar's magnetospheric parameters even very energetic electrons are unable to produce the observed photon energies.

It is generally accepted, that the X-ray spectra of RXJ1856 and RBS1774 are purely thermal and is best represented by a Planckian shape. A fit of the Chandra LETGS X-ray spectrum of RXJ1856 with a blackbody model, absorbed by cold interstellar matter gives $\chi^2 = 1.2$ (Burwitz et al., 2003). And when the fitting is done with our model the resulting $\chi^2 = 1.00$ (see the fitting results in Tab.4.1). For RBS1774 a fit with a pure blackbody component absorbed by cold interstellar matter gives $\chi^2 = 1.81$ (Schwope et al., 2009). Including a Gaussian absorption line at $\sim 0.7\text{keV}$ (as the largest discrepancies between model and data are around 0.7keV) improves the fit $\chi^2 = 1.50$ (parameters are listed in Tab.4.2). The fit with a model spectrum absorbed by cold interstellar matter yields $\chi^2 = 1.63$, and including an absorption edge improves the fit leading to a reduced $\chi^2 = 1.50$. The best-fitting energy of the edge is $E_{edge} = 0.679\text{keV}$, and the optical depth is $\tau_{edge} = 0.20$. These objects are strongly believed to be the sources of the pure thermal emission, as their X-ray spectra are best represented by simple Planckian function and there is no sign of any non-thermal X-ray power-law such as those seen in the spectra of most radio pulsars. But as we see, our model gives the synchrotron spectral distribution (a power-law with exponential cutoff) which represents the observational data as well as the Planckian function. Thus, this argument is not enough to conclude that these objects are purely thermal sources.

We suppose that the most reliable argument revealing the real emission nature of RXJ1856 and RBS1774 will be the study of these object with polarization instruments. In case of RXJ1856, if the emission of this source has a thermal nature, then according to Ho (2007) (this model gives the best match of the entire spectrum, among other thermal emission models) the X-ray emission should be linearly polarized with the polarization degree equal to 100%. The position angle should undergo small changes for the case of

($2^\circ, 30^\circ$) and for the case of ($30^\circ, 2^\circ$) it should rotate by 360° in one observable pulse (where these quantities are the possible angles between the rotation and the magnetic pole axes and between the rotation and the observer's axes). But if the emission of this source is generated by the synchrotron mechanism, it is expected that the X-ray emission will be linearly polarized with the frequency dependent polarization degree, giving the values from a few percent up to 84%.

The nature of the spectral feature detected in X-ray spectrum of RBS1774 is not fully clarified as yet. The most likely interpretation is that it is due to proton cyclotron resonance, which implies ultrastrong magnetic field of $B_{cyc} \sim 10^{14}\text{G}$ (Zane et al., 2005; Rea et al., 2007). Although, the required strong magnetic field is inconsistent with timing measurements giving $B_{dip} = 3.2 \cdot 10^{19} \sqrt{P\dot{P}} \simeq 2 \cdot 10^{13}\text{G}$ (Kaplan & van Kerkwijk, 2009). We suppose that existence of the absorption feature in spectra of RBS1774 is caused by wave damping at photon energies $\sim 0.7\text{keV}$, which takes place near the light cylinder. During the farther motion in the pulsar magnetosphere, the X-ray emission of RBS1774 comes in the cyclotron damping range (see Eq. (5.5)). If we assume that damping happens on the left slope of the distribution function of primary beam electrons (see Fig. 2.1), then the photon energy of damped waves will be $\epsilon_0 = (h/2\pi)\omega_0 = (h/2\pi)2\omega_B/\gamma_b\psi^2 \simeq 0.7\text{keV}$. Taking into account the shape of the distribution function of beam electrons, we interpret the large residuals around $\sim 0.7\text{keV}$ (see Fig. 4.2) as an absorption edge. Including an absorption edge improves the fit leading to a reduced $\chi^2 = 1.50$. The best-fitting energy of the edge is $E_{edge} = 0.679\text{keV}$, and the optical depth is $\tau_{edge} = 0.20$ (see Tab.4.2). However, adding an absorption edge to the model spectrum does not produce a statistically significant improvement of the fitting. According to Schwobe et al. (2009) if one uses the RGS X-ray spectra of RBS1774 in place of EPIC spectra, the resulting χ^2 is changed just marginally when a Gaussian absorption line is included at $\sim 0.7\text{keV}$. Thus, we conclude that the nature of the feature at 0.7keV is uncertain and might be related to calibration uncertainties of the CCDs and the RGS at those very soft X-ray energies. The same can be told about a feature at $\sim 0.3\text{keV}$

(the large residuals around 0.3keV are evident from inspection of Fig. 4.2 and 4.3). A feature of possible similar nature was detected in EPIC-pn spectra of the much brighter prototypical object RXJ1856.4-3754 and classified as remaining calibration problem by Haberl (2007). Consequently, more data are necessary to finally prove or disprove the existence of those features.

The frequency of the original waves, excited during the cyclotron resonance can be estimated from Eq. (2.16) as follows $\nu \approx 2\pi\omega_B/\delta\gamma_b \sim 10^{14}\text{Hz}$. As we can see the frequency of cyclotron modes comes in the same domain as the measured optical emission of RBS1774 and RXJ1856 (Zane et al., 2008; Schwope et al., 2009; Burwitz et al., 2003).

The effectiveness of the cyclotron mechanism has been estimated and it appears to be quite efficient. For effective generation of waves it is essential that the time during which the particles give energy to waves should be more than $1/\Gamma_c$. The optical waves propagate practically in straight lines, whereas the dipolar magnetic field lines deviate from their initial direction, and the angle $\alpha = k_{\parallel}/k_{\varphi}$ grows. On the other hand, the resonance condition (2.16) imposes limitations on α i.e. particles can resonate with the waves propagating in a limited range of angles. The estimations show that in our case, the fulfillment of $\rho \gtrsim 3 \cdot 10^9\text{cm}$ implies an effectiveness of the cyclotron mechanism. As the instability develops at distances $r \sim 10^9\text{cm}$, it follows that the excited waves lie in the resonant region long enough for particles to acquire pitch angles and to generate the observed radiation.

The recently discovered 7s pulsations of the X-ray emission of RXJ1856 has been explained in the framework of the drift wave driven model. The main feature of this model is that the spin period of the pulsar might differ from the observable period (for RXJ1856 the real spin period is estimated to be $\sim 1\text{s}$), as a consequence of the existence of very low frequency drift waves in the region of generation of the pulsar emission. These particular waves are not detected but only result in a periodic change of curvature of the magnetic field lines, which in turn cause the change of observed radiation with a period of the drift wave.

The only test to find out if the observed pulse period is a 'real' spin period

or a period of the drift wave is to observe the behaviour of the position angle. The position angle should rotate by 360° within one 'real' pulse supposed to be of the order of 1 s. It should undergo full circular rotation several times within the observable period of 7.055s.

Appendix

Curvature drift instability

In this section we study the process of straightening the magnetic field lines out due to the parametrically excited CDI (this particular problem was considered in Machabeli & Osmanov (2010)). This instability is called parametric, because an external force - centrifugal force, plays a role of a parameter, that changes in time and creates the instability. Generally speaking, the presence of an external varying parameter generates the plasma instability. The mechanism of energy pumping process from the external alternating electric field into the electron-ion plasma is quite well investigated in (Silin, 1973; Galeev & Sagdeev, 1973; Max, 1973). Instead of considering the altering electric field, one can examine the centrifugal force as a varying parameter (Machabeli et al., 2005).

We start our consideration by supposing that the magnetic field lines are almost straight with very small nonzero curvature (see Fig. 1). In this context we examine the field lines that are open, and thus have the curvature radius exceeding the light cylinder one, maximum by one order. Therefore, dynamics of particles, governing the overall picture of the CDI, can be studied, assuming that field lines are almost straight. It is well known that the dynamics of plasma particles moving along the straight co-rotating magnetic field lines is described by the Euler equation: (Machabeli et al., 2005):

$$\frac{\partial \mathbf{p}_\alpha}{\partial t} + (\mathbf{v}_\alpha \nabla) \mathbf{p}_\alpha = -c^2 \gamma_\alpha \xi \nabla \xi + \frac{e_\alpha}{m} \left(\mathbf{E} + \frac{1}{c} \mathbf{v}_\alpha \times \mathbf{B} \right), \quad (1)$$

where $\xi \equiv \sqrt{1 - \Omega^2 R^2 / c^2}$, R is the coordinate along the straight field lines; \mathbf{p}_α , \mathbf{v}_α , and e_α are the momentum (normalized to the particle's mass), the

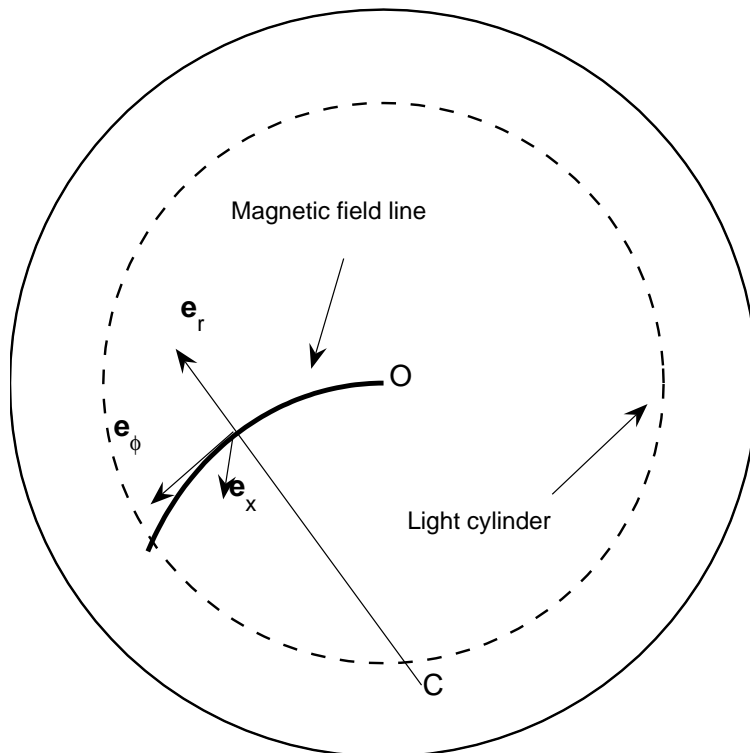


Figure 1: Here we show geometry in which we consider our system of equations. By e_ϕ , e_r and e_x unit vectors are denoted, note that $e_x \perp e_{\phi,x}$. O is the center of rotation and C - the curvature center.

velocity and the charge of electrons/positrons, respectively; $\alpha = \{e^\pm, b\}$ denotes the sort of particles and \mathbf{E} and \mathbf{B} are the electric and the magnetic field induction respectively. The continuity equation:

$$\frac{\partial n_\alpha}{\partial t} + \nabla(n_\alpha \mathbf{v}_\alpha) = 0, \quad (2)$$

and the induction equation:

$$\nabla \times \mathbf{B} = \frac{1}{c} \frac{\partial \mathbf{E}}{\partial t} + \frac{4\pi}{c} \sum_{\alpha=e^\pm, b} \mathbf{J}_\alpha, \quad (3)$$

(where n_α and \mathbf{J}_α are the density and the current, respectively) complete the set of equations for n , \mathbf{v} , \mathbf{E} and \mathbf{B} .

In the leading state the plasma is in the frozen-in condition: $\mathbf{E}_0 + \frac{1}{c} \mathbf{v}_0 \times \mathbf{B}_0 = 0$, then, one can show that the solution to the Euler equation in Eq. (1) for ultra relativistic particle velocities in the leading state is given by

(Machabeli & Rogava, 1994):

$$v_\theta^0 \equiv v_\parallel = c \cos(\Omega t + \varphi), \quad (4)$$

where v_\parallel is the velocity component along the magnetic field lines and φ is the initial phase of each particle.

For solving the set of Eqs. (1-3), we will linearize it assuming that, in the zeroth order of approximation, the flow has the longitudinal velocity satisfying Eq. (4) and also drifts along the x -axis driven by the curvature of magnetic field lines (see Fig. 1):

$$u_\alpha = \frac{\gamma_{\alpha_0} v_\parallel^2}{\omega_{B_\alpha} \rho}, \quad (5)$$

where u_α is the drift velocity; $\omega_{B_\alpha} = e_\alpha B_0 / mc$; and B_0 is the background magnetic induction.

Let us expand the physical quantities up to the first order terms:

$$\Psi \approx \Psi^0 + \Psi^1, \quad (6)$$

where $\Psi \equiv \{n, \mathbf{v}, \mathbf{p}, \mathbf{E}, \mathbf{B}\}$. Then if we examine only the x components of Eqs. (1) and (3), and express the perturbed quantities as follows:

$$\Psi^1(t, \mathbf{r}) \propto \Psi^1(t) \exp [i(\mathbf{k}\mathbf{r})], \quad (7)$$

by taking into account that $k_\theta \ll k_x$ and $k_r = 0$, and bearing in mind that $v_r^1 \approx cE_x^1/B_0$, one can show that Eqs. (1-3) reduce to the form:

$$\frac{\partial p_{\alpha_x}^1}{\partial t} - i(k_x u_\alpha + k_\theta v_\parallel) p_{\alpha_x}^1 = \frac{e_\alpha}{mc} v_\parallel B_r^1, \quad (8)$$

$$\frac{\partial n_\alpha^1}{\partial t} - i(k_x u_\alpha + k_\theta v_\parallel) n_\alpha^1 = ik_x n_\alpha^0 v_{\alpha_x}^1, \quad (9)$$

$$-ik_\theta c B_r^1 = 4\pi \sum_{\alpha=e^\pm, b} e_\alpha (n_\alpha^0 v_{\alpha_x}^1 + n_\alpha^1 u_\alpha). \quad (10)$$

According to the standard method (see Osmanov et al., 2008), after express-

ing $v_{\alpha_x}^1$ and n_α^1 in the following way:

$$v_{\alpha_x}^1 \equiv V_{\alpha_x} e^{i\mathbf{k}\mathbf{A}_\alpha(t)}, \quad (11)$$

$$n_\alpha^1 \equiv N_\alpha e^{i\mathbf{k}\mathbf{A}_\alpha(t)}, \quad (12)$$

$$A_{\alpha_x}(t) = \frac{u_\alpha}{2\Omega} (\Omega t + \varphi) + \frac{u_\alpha}{4\Omega} \sin[2(\Omega t + \varphi)], \quad (13)$$

$$A_{\alpha_\theta}(t) = \frac{c}{\Omega} \sin(\Omega t + \varphi), \quad (14)$$

and substituting them into Eqs. (8,9), one can get the expressions:

$$v_{\alpha_x}^1 = \frac{e_\alpha}{mc\gamma_{\alpha_0}} e^{i\mathbf{k}\mathbf{A}_\alpha(t)} \int^t e^{-i\mathbf{k}\mathbf{A}_\alpha(t')} v_{\parallel}(t') B_r(t') dt', \quad (15)$$

$$n_\alpha^1 = \frac{ie_\alpha n_\alpha^0 k_x}{mc\gamma_{\alpha_0}} e^{i\mathbf{k}\mathbf{A}_\alpha(t)} \int^t dt' \int^{t''} e^{-i\mathbf{k}\mathbf{A}_\alpha(t'')} v_{\parallel}(t'') B_r(t'') dt'', \quad (16)$$

which combined with Eq. (10), lead to the following form:

$$\begin{aligned} -ik_\theta c B_r^1(t) &= \sum_{\alpha=e^\pm, b} \frac{\omega_\alpha^2}{\gamma_{\alpha_0} c} e^{i\mathbf{k}\mathbf{A}_\alpha(t)} \int^t e^{-i\mathbf{k}\mathbf{A}_\alpha(t')} v_{\parallel}(t') B_r(t') dt' + \\ i \sum_{\alpha=e^\pm, b} \frac{\omega_\alpha^2}{\gamma_{\alpha_0} c} k_x u_\alpha e^{i\mathbf{k}\mathbf{A}_\alpha(t)} &\int^t dt' \int^{t''} e^{-i\mathbf{k}\mathbf{A}_\alpha(t'')} v_{\parallel}(t'') B_r(t'') dt'', \end{aligned} \quad (17)$$

where $\omega_\alpha = e\sqrt{4\pi n_\alpha^0/m}$ represents the plasma frequency. If we apply the following identity:

$$e^{\pm ix \sin y} = \sum_s J_s(x) e^{\pm isy}, \quad (18)$$

to Eq. (17), the latter will simplify to the following form:

$$\begin{aligned} B_r(\omega) &= - \sum_{\alpha=e^\pm, b} \frac{\omega_\alpha^2}{2\gamma_{\alpha_0} k_\theta c} \sum_{\sigma=\pm 1} \sum_{s, n, l, p} \frac{J_s(g_\alpha) J_n(h) J_l(g_\alpha) J_p(h)}{\omega + \frac{k_x u_\alpha}{2} + \Omega(2s + n)} \times \\ &\times B_r(\omega + \Omega(2[s - l] + n - p + \sigma)) \left[1 - \frac{k_x u_\alpha}{\omega + \frac{k_x u_\alpha}{2} + \Omega(2s + n)} \right] \times \\ &\times e^{i\varphi(2[s-l]+n-p+\sigma)} + \end{aligned}$$

$$\begin{aligned}
& + \sum_{\alpha=e^{\pm},b} \frac{\omega_{\alpha}^2 k_x u_{\alpha}}{4\gamma_{\alpha_0} k_{\theta} c} \sum_{\sigma,\mu=\pm 1} \sum_{s,n,l,p} \frac{J_s(g_{\alpha}) J_n(h) J_l(g_{\alpha}) J_p(h)}{\left(\omega + \frac{k_x u_{\alpha}}{2} + \Omega(2[s + \mu] + n)\right)^2} \times \\
& \times B_r(\omega + \Omega(2[s - l + \mu] + n - p + \sigma)) \times e^{i\varphi(2[s-l+\mu]+n-p+\sigma)}, \quad (19)
\end{aligned}$$

where

$$g_{\alpha} = \frac{k_x u_{\alpha}}{4\Omega}, \quad h = \frac{k_{\theta} c}{\Omega}$$

and $J_s(x)$ ($s = 0; \pm 1; \pm 2 \dots$) is the Bessel function of integer order (Abramovitz & Stegan, 1965).

In order to solve Eq. (19), one has to examine similar equations, rewriting Eq. (19) (with shifted arguments) for $B_r(\omega \pm \Omega)$, $B_r(\omega \pm 2\Omega)$, etc.. This implies that we have to solve the system with the infinite number of equations, making the problem impossible to handle. Therefore, the only way is to consider the physics close to the resonance condition, that provides the cutoff of the infinite row in Eq. (19) and makes the problem solvable (Silin & Tikhonchuk, 1970).

Studying the resonance state of our physical system (see Eq. (19)), one can derive the proper frequency for the CDI:

$$\omega_0 \approx -\frac{k_x u_{\alpha}}{2}. \quad (20)$$

The present condition for physically meaningful case $k_x u_{\alpha}/2 < 0$ implies that $2s + n = 0$ and $2[s + \mu] + n = 0$ when $\omega_0 \ll \Omega$.

For solving Eq. (19), we examine the average value of B_r with respect to φ . Then, by taking into account the formula:

$$\frac{1}{2\pi} \int e^{iN\varphi} d\varphi = \delta_{N,0},$$

and preserving only the leading terms of Eq. (19), after neglecting the contribution from the plasma components, one can derive the dispersion relation for the instability (see Osmanov et al., 2008):

$$\left(\omega + \frac{k_x u_b}{2}\right)^2 \approx \frac{3\omega_b^2 k_x u_b}{2\gamma_{b_0} k_{\theta} c}. \quad (21)$$

By expressing the frequency as $\omega \equiv \omega_0 + i\Gamma$ it is easy to estimate the increment of the CDI:

$$\Gamma \approx \left(-\frac{3}{2} \frac{\omega_b^2}{\gamma_{b0}} \frac{k_x u_b}{k_{\theta c}} \right)^{1/2} \left| J_0 \left(\frac{k_x u_b}{4\Omega} \right) J_0 \left(\frac{k_{\theta c}}{\Omega} \right) \right|. \quad (22)$$

Bibliography

- [1] Abramovitz, M. & Stegun, I., 1965, Handbook of Mathematical Functions, (eds.: Dover Publications Inc.: New York), p. 320
- [2] Akhiezer A.I., 1967, Collective oscillations in a plasma, M.I.T. Press (1967)
- [3] Aliu E. et al., 2008, Sci, 322, 1221A
- [4] Arons J. & Scharleman E.T., 1979, ApJ, 231, 854
- [5] Arons, J. 1981, In: Proc. Varenna Summer School and Workshop on Plasma Astrophysics, ESA, p.273
- [6] Arons, J., & Barnard, J. J., ApJ, 302, 120
- [7] Artsimovich L.A. & Sagdeev R.Z., 1979, Plasma physics for physicists, (russian edition) Moscow, Atomizdat
- [8] Bekefi George & Barrett Alan H., 1977, Electromagnetic vibrations, waves and radiation, The MIT Press, Cambridge, Massachusetts and London, England
- [9] Bellazzini, R., et al. 2006, preprint (astro-ph/0609571)
- [10] Blandford R.D., Netzer H. & Woltjer L., 1990, Active Galactic Nuclei, Springer-Verlag
- [11] Braje, T. M., Romani, R. W., 2002, ApJ, 580, 1043
- [12] Burwitz, V., Zavlin, V. E., Neuhäuser, R., Predehl, P., Trümper, J. Brinkman, A. C., 2001, A&A, 379, L35
- [13] Burwitz, V., Haberl, F. Neuhäuser, R., Predehl, P., Trümper, J. Zavlin, V. E., 2003, A&A, 399, 1109

- [14] Chkheidze, N., Machabeli, G., 2007, *A&A*, 471, 599
- [15] Chkheidze, N., Lomiashvili, D., 2008, *NewA*, 13, 12
- [16] Chkheidze, N., 2009, *A&A*, 500, 861
- [17] Chkheidze, N., Machabeli, G., Osmanov, Z., 2010, *ApJ*, (Accepted)
- [18] Chkheidze, N., 2011, *A&A*, 527A, 2C
- [19] Collins, G. W., II, Claspy, W. P., & Martin, J. C. 1999, *PASP*, 111, 871
- [20] Daugherty, J. K., & Harding, A. K., 1982, *ApJ*, 252, 33
- [21] Dickey, J., & Lockman, F. 1990, *ARA&A*, 28, 215
- [22] Dombrovsky, V. A., 1954, *Dokl. Akad. Nauk SSSR*, 94, 1021
- [23] Drake, J. J., Marshall, H. L., Dreizler, S., Freeman, P. E., Fruscione, A., et al. 2002, *ApJ*, 572, 996
- [24] Elvis, M. 2006, in *Space Telescopes and Instrumentation II: Ultraviolet to Gamma Ray*, eds. M.J.L. Turner & G. Hasinger, *Proceedings of the SPIE*, 6266, 62660Q
- [25] Galeev, A. A., & Sagdeev, R. Z., 1973, *Nucl. Fusion*, 13, 603
- [26] Ginzburg, V. L., "Teoreticheskaia Fizika i Astrofizika" ,Nauka, Moskva 1981
- [27] Gold, T., 1969, *Nature*, 218, 731
- [28] Goldreich, P., Julian, W. H., 1969, *ApJ*, 157, 869
- [29] Gwinn, C., et al. 1997, *ApJ*, 483, L53
- [30] Haberl, F., 2007, *Ap&SS*, 308, 181
- [31] Harding A.K., Stern J.V., Dyks J. & Frackowiak M., 2008, *ApJ*, 680, 1378
- [32] Hewish A. et al. *Nature*, 217, 709, 1968

- [33] Ho, W. C. G., Kaplan, D. L., Chang, P., Adelsberg, M., Potekhin, A. Y., 2007, MNRAS 375, 281H
- [34] Jahoda, K., Black, K., Deines-Jones, P., Hill, J.E., Kallman, T., Strohmayer, T., & Swank, J. 2007, preprint (astro-ph/0701090)
- [35] Ho, W. C. G., 2007, MNRAS 380, 71H
- [36] Kaplan, D.L., Kulkarni, S., Van Kerkwijk, M.H. 2003, ApJ, 588, L33
- [37] Kaplan, D.L. 2008, proceedings of 40 Years of Pulsars: Millisecond Pulsars, Magnetars, and More, August 12-17, 2007, McGill University, Montreal, Canada, AIP, 983, 331
- [38] Kaplan, D. L., van Kerkwijk, M. H., 2009, ApJ, 692, 62
- [39] Kazbegi A. Z., Machabeli G. Z., Melikidze G. I., 1991, MNRAS, 253, 377
- [40] Kazbegi A. Z., Machabeli G. Z., Melikidze G. I., 1991b, Austral. J. Phys., 44, 573
- [41] Kazbegi A.Z., Machabeli G.Z & Melikidze G.I., 1992, in Proc. IAU Collog. 128, The Magnetospheric Structure and Emission Mechanisms of Radio Pulsars, ed. T.H. Hankins, J.M. Rankin & J.A. Gil (Zielona Gora: Pedagogical Univ. Press), 232
- [42] Kazbegi A. Z., Machabeli G. Z., Melikidze G. I., Shukre C., 1996, A&A, 309, 515
- [43] Kawamura, K., & Suzuki, I., 1977, Astrophys. J., 217, 832
- [44] Khechinashvili, D. G., Melikidze, G. I., 1997, A&A, 320, L45
- [45] Knude, J., & Hog, E., 1998, A&A 338, 897
- [46] Lai, D., Salpeter, E. E., 1997, ApJ, 491, 270
- [47] Lai, D., 2001, Rev. of Mod. Phys. 73, 629
- [48] Landau L.D. & Lifshitz E.M., 1971, Classical Theory of Fields (London: Pergamon)

- [49] Lesch, H., Kramer, M., & Kunzl, T. 1998, *A&A*, 323, L21
- [50] Lessard, R. W., et al., 2000, *ApJ*, 531, 942
- [51] Lomiashvili D., Machabeli G., & Malov I., 2006, *ApJ*, 637, 1010
- [52] Lominadze, D. G., Machabeli, G. Z., and Mikhailovskii, A. B., 1979, *Fiz. Plaz.*, 5, 1337
- [53] Lominadze J.G., Machabeli G. Z., & Usov V. V., 1983, *Ap&SS*, 90, 19L
- [54] Lominadze, J. G., Machabeli, G. Z., Melikidze, G. I., & Pataraiia, A. D., 1986, *Sov. J. Plasma Phys.*, 12, 712
- [55] Lyutikov M., Machabeli G. & Blandford R., 1999, *ApJ*, 512, 804
- [56] Lyutikov, M., Blandford, R. D., Machabeli, G. Z., 1999, *MNRAS* 305, 338L
- [57] Machabeli, G. Z., & Usov, V. V., 1979 *AZh Pi'sma*, 5, 445
- [58] Machabeli G., Osmanov Z. & Mahajan S., 2005, *Phys. Plasmas* 12, 062901
- [59] Machabeli, G. Z., Luo, Q., Vladimirov, S. V., & Melrose, D. B., 2002, *Phys. Rev. E*, 65, 036408
- [60] Machabeli G. & Osmanov Z., 2009, *ApJL*, 700, 114
- [61] Machabeli G. & Osmanov Z., 2010, *ApJ*, 709, 547
- [62] Machabeli, G.Z. & Rogava, A. D., 1994, *Phys.Rev. A*, 50, 98
- [63] Malov, I, F., Machabeli, G. Z., 2002, *Astronomy Reports*, Vol. 46, Issue 8, p.684
- [64] Manchester R.N. & Taylor J.H., 1980, *Pulsars*, F.H. Freeman and Company
- [65] Malov, I. F., Machabeli, G. Z., 2007, *Ap&SS*, 29M
- Max C., 1973, *Phys. Fluids*, 16, 1480

- [66] Melrose D.B. & McPhedran R.C., 1991, *Electromagnetic Processes in Dispersive Media*, Cambridge University Press (September 27, 1991)
- [67] Melrose, D. B. 1995, *A&A*, 16, 137
- [68] Motch, C., Zavlin, V. E., & Haberl, F. 2003, *A&A*, 408, 323
- [69] Motch, C., et al. 2005, *A&A*, 429, 257
- [70] Muslimov A.G. & Tsygan A.I., 1992, *MNRAS*, 255, 61
- [71] Neuhäuser, R., Thomas, H. C., & Walter, F. M. 1998, *The Messenger*, 92, 27
- [72] Neuhäuser, R. 2001, *AN*, 322, 3
- [73] Oort, J. H., & Walraven, T. 1956, *Bull. Astron. Inst. Netherlands*12, 285
- [74] Osmanov Z., Rogava A.S. & Bodo G., 2007, *A&A*, 470, 395
- [75] Osmanov, Z., Shapakidze, D., & Machbeli, G., 2009a, *A&A*, 509, 19
- [76] Osmanov, Z., Shapakidze, D. & Machabeli, G. 2009b, *A&A*, 503, 19
- [77] Osmanov, Z., Dalakishvili, G. & Machabeli, G., 2008, *MNRAS*, 383, 1007
- [78] Pacini F., 1971, *ApJ*, 163, 117
- [79] Pacholczyk, A. G. 1970, *Radio Astrophysics* (San Francisco: W. H. Freeman)
- [80] Paerels, F., Mori, K., Motch, C., et al., 2001, *A&A*, 365, L298
- [81] Pavlov, G. G., Zavlin, V. E., Trümper, J., Neuhäuser, R., 1996, *ApJ*, 472, L33
- [82] Pavlov, G. G., 2000, Talk at the ITP/UCSB workshop "Spin and Magnetism of Young Neutron Stars"
- [83] Pavlov, G. G., Zavlin, V. E., Sanwal, D., in *Neutron Stars and Supernova Remnants*. Eds. W. Becher, H. Lesch, & J. Trümper, 2002, *MPE Report* 278, 273

- [84] Pons, J. A., Walter, F. M., Lattimer, J. M., Prakash, M., Neuhaäuser, R., An, P., 2002, *ApJ*, 564, 981
- [85] Rajagopal, M., Romani, R. W., Miller, M. C., 1997, *ApJ*, 479, 347
- [86] Rankin, J. M., 1983, *ApJ*, 274, 333
- [87] Ransom, S. M., Gaensler, B. M., Slane, P.O. 2002, *ApJ*, 570, L75
- [88] Rea, N. er al. 2007, *MNRAS*, 379, 1484
- [89] Rogava A. D., Dalakishvili G. & Osmanov Z., 2003, *Gen. Relativ. Gravit.* 35, 1133
- [90] Romani, R. W., & Yadigaroglu, I. A., 1995, *ApJ*, 438, 31
- [91] Ruderman M.A. & Sutherland P.G., 1975, *ApJ*, 196, 51
- [92] Rutledge, R. E., Fox, D. W., Bogosavljevic, M. and Mahabal, A., 2003, *ApJ* 598, 458
- [93] Rybicki G.B. & Lightman A. P., 1979, *Radiative Processes in Astrophysics*. Wiley, New York
- [94] Sagdeev, R. S., & Shafranov, V. D., 1960, *Zh. Eksp. Teor. Fiz.*, 39, 181
- [95] Schwope, A. D., Erben, T., Kohnert, J., Lamer, G., Steinmetz, M., et al. 2009, *A&A*, 499, 267S
- [96] Shapakidze D., Machabeli G., Melikidze G. & Khechinashvili D., 2003, *Phys. Rev. E.*, id. 026407
- [97] Shklovsky, I. S., 1953, *ApJ*, 123, 498
- [98] Silin V.P. & Tikhonchuk V.T., 1970, *J. Appl. Mech. Tech. Phys.*, 11, 922
- [99] Silin V.P., 1973, 'Parametricheskoe Vozdeistvie izluchenija bol'shoj mosshnosti na plazmu', Nauka, Moskva
- [100] Sturrock P. A., 1971, *ApJ*, 164, 529
- [101] Tademaru E., 1973, *ApJ*, **183**, 625

- [102] Tiengo, A., Mereghetti, S., 2007, ApJ, 657, L101
- [103] Treves, A., Turolla, R., Zane, S., & Colpi, M. 2000, PASP, 112, 297
- [104] Turolla, R., Zane, S. Drake, J. J., 2004, ApJ, 603, 265
- [105] van Kerkwijk, M. H., Kaplan, D. L., 2008, ApJ, 637L, 163V
- [106] Usov V.V., Shabad A., 1985, Ap&SS, 117, 309
- [107] Vashakidze, M. A., 1954, Astron. Tsirk., 149, 11
- [108] Vedenov A.A., Velikhov E.P. & Sagdeev R.Z., 1961, Soviet Physics Uspekhi, Volume 4, Issue 2, 332
- [109] Voges, W. et al., 1999, A&A 349, 389
- [110] Volokitin, A. S., Krasnoselskikh, V. V., & Machabeli, G. Z., 1985, Sov. J. Plasma Phys., 11, 310
- [111] Walter, F. M., Wolk, S. J., Neuhäuser, R., 1996, Nature 379,233
- [112] Walter, F. M., & Matthews, L. D. 1997, Nature, 389, 358
- [113] Walter, F. M. 2001, ApJ, 549, 433
- [114] Weekes, T. C., et al. 1989, ApJ, 342, 379
- [115] Zampieri, L., et al. 2001, A&A, 378, L5
- [116] Zane, S., Cropper,M., Turolla, R., et al. 2005, ApJ, 627, 397
- [117] Zane, S., et al. 2006, A&A, 570, 619
- [118] Zane, S., et al. 2008, ApJ, 682, 487
- [119] Zakharov V.E., 1972, JETP, 35, 908
- [120] Zavlin, V. E., Pavlov, G. G., 2002 in Neutron Stars and Supernova Remnants, Eds. Becker, W., Lesch, H., Trümper, J., MPE Report 278, p.261
- [121] Zhelezniakov, V. V., "Volni v Kosmicheskoi Plazme" Nauka, Moskva 1977